The Distribution of the Hydroxyl Radical in the Troposphere

By
Jack Fishman
Paul J. Crutzen

Department of Atmospheric Science
Colorado State University
Fort Collins, Colorado

Colorado State University

Department of Atmospheric Science

Paper No. 284

THE DISTRIBUTION OF THE HYDROXYL RADICAL IN THE TROPOSPHERE

by

Jack Fishman

and

Paul J. Crutzen

Preparation of this report
has been financially supported by
Environmental Protection Agency
Grant No. R804921-01

Department of Atmospheric Science
Colorado State University
Fort Collins, Colorado

January, 1978

Atmospheric Science Paper No. 284

Abstract

A quasi-steady state photochemical numerical model is developed to calculate a two-dimensional distribution of the hydroxyl (OH) radical in the troposphere. The diurnally, seasonally averaged global value of OH derived by this model is 3×10^5 cm^{-3} which is several times lower than the number computed previously by other models, but is in good agreement with the value inferred from the analysis of the tropospheric distribution of methyl chloroform. Likewise, the effects of the computed OH distribution on the tropospheric budgets of ozone and carbon monoxide are not inconsistent with this lower computed value.

One important result of this research is the detailed analysis of the distribution of tropospheric ozone in the Southern Hemisphere. Our work shows that there is a considerable difference in the tropospheric ozone patterns of the two hemispheres and that through the analysis of the likely photochemistry occurring in the troposphere, a significant source of tropospheric ozone may exist in the Northern Hemisphere due to carbon monoxide oxidation. Future research efforts will be devoted to the meteorological dynamics of the two hemispheres to try to distinguish if these physical processes are similarly able to explain the interhemispheric differences in tropospheric ozone.

As a result of the lesser amount of ozone found in the Southern Hemisphere troposphere, our calculations do not indicate that there should be substantially higher concentrations of OH in that hemisphere as had been previously speculated (Crutzen and Fishman, 1977; Singh, 1977b).

By performing a sensitivity study on the budgets of tropospheric ozone and carbon monoxide, our model results indicate that there should be very low background concentrations of the nitrogen oxides (NO and NO_2) in the troposphere. In addition, a relatively fast heterogeneous removal rate for several gases (e.g., hydrogen peroxide and nitric acid) is most likely necessary to obtain an understanding of the overall photochemistry occurring in the troposphere.

Table of Contents

Acknowledgements

We wish to thank Susan Solomon of the Department of Chemistry, University of California, Berkeley, for her help in the analysis of the Southern Hemisphere tropospheric ozone data which played an integral part in the formulation of this report. Susan worked with us at the National Center for Atmospheric Research (NCAR) in Boulder, Colorado, as a UCAR (University Corporation for Atmospheric Research) Fellowship Participant during the Summer of 1977. We also acknowledge the cooperation of Russ Dickerson and Donald Stedman, both of the Department of Chemistry at the University of Michigan, who made available to us some of their preliminary data for comparison in this report. The clerical competence of Julie Wilson is also much appreciated.

The computations for this study were performed at the NCAR Computing Facility in cooperation with the Air Quality Division of NCAR.

This research was partially funded by Environmental Protection Agency Grant R804921-01.

I. INTRODUCTION

The abundance of the hydroxyl (OH) radical in the troposphere is one of the primary factors to be considered in the determination of the removal rate of many trace gases in this region. In addition to attacking naturally-occurring species such as methane, OH reactions likewise provide the major sink for many anthropogenically released compounds. In particular, most of the chlorine contained in many commonly used chlorocarbon chemicals (e.g., methyl chloroform, perchloroethylene, etc.) is believed to be removed in the troposphere through reaction sequences initiated by hydroxyl radical attack. If these chemicals did diffuse into the stratosphere, ultraviolet radiation could photolyze them where free chlorine atoms (products of the photolysis) could cause catalytic destruction of ozone through the sequence (e.g., see Stolarski and Cicerone, 1974; Molina and Rowland, 1974; Crutzen et al., 1977):

$$\begin{aligned} Cl + O_3 &\rightarrow ClO + O_2 \\ ClO + O &\rightarrow Cl + O_2 \\ \hline O_3 + O &\rightarrow 2O_2. \end{aligned}$$

This discussion focuses on the global distribution of OH in the troposphere and its relevance to the fates of several industrially released chemicals. Whereas previously accepted estimates of average OH concentration have been on the order of 10 to 30 x 10^5 cm^{-3} (see Singh, 1977a), the results computed by the model described in this study calculated average OH concentrations on the order of 3 x 10^5 cm^{-3}. This number is consistent with the calculations derived in consideration of the CO budget (Crutzen and Fishman, 1977), and the tropospheric methyl chloroform (CH_3CCl_3)

distribution (Singh, 1977a). Although budget considerations of the above gases support the lower OH concentrations presented in this study, direct computation using available photokinetic information had always suggested the higher OH concentrations (e.g., Levy, 1972, 1973; Chang and Wuebbles, 1976).

The lower computed hydroxyl radical number densities are partially the result of some new information about quantum yields and reaction rate kinetics which influence OH directly. The experiments by Cox et al. (1976a), Sie et al. (1976) and Chan et al. (1977) have shown that the primary removal process of OH in the atmosphere,

$$CO + OH \rightarrow CO_2 + H,$$

exhibits a pressure dependence. In particular, Chan et al. (1977) give a reaction rate constant at lower tropospheric pressures ($\sim$1 atm) which is more than twice that which was previously accepted (Hampson and Garvin, 1975). Furthermore, recent laboratory studies (Arnold et al., 1977; Moortgat et al., 1977) also have shown that the quantum yield of metastable atomic oxygen, $O(^1D)$ from ozone photolysis between 300 and 320 nm decreases with lower temperature. Previously, calculations had been carried out with quantum yield data found at room temperature (e.g., Moortgat and Warneck, 1975). In the following sections, the effects of these new data as well as some other factors which influence OH radical number density in the troposphere will be examined. The composition of the troposphere being considered in this study does not include the photochemistry of hydrocarbons other than methane and the products of methane oxidation. Future modelling efforts tentatively will include these more complex

molecules and will examine their roles in the distribution of OH and the budgets of ozone and carbon monoxide.

II. THE PHOTOCHEMISTRY OF ODD HYDROGEN RADICALS

The odd hydrogen radicals in the troposphere consist primarily of the hydroxyl (OH) radical and the perhydroxyl (HO_2) radical. These reactants exist only during daytime since they are formed either by photolysis or by reactions involving very short-lived products of photolysis. The odd hydrogen radical-producing reactions considered in these calculations are:

R1 $H_2O + O(^1D) \rightarrow 2\ OH$

R2 $H_2 + O(^1D) \rightarrow H + OH$

R3 $CH_4 + O(^1D) \rightarrow CH_3 + OH$

R5 $CH_3OOH + h\nu \rightarrow CH_3O + OH$

R8 $CH_3O + O_2 \rightarrow CH_2O + HO_2$

R7a $CH_2O + h\nu \rightarrow CHO + H$

R4 $H_2O_2 + h\nu \rightarrow 2\ OH$

and R6 $HNO_3 + h\nu \rightarrow NO_2 + OH.$

Upon examination of the above reactions, two important points must be emphasized. First of all, the production of formyl radicals, CHO, and hydrogen atoms, H, are considered as production of perhydroxyl radicals since the recombination of these species with an oxygen molecule is assumed to proceed instantaneously:

R31 $HCO + O_2 \rightarrow CO + HO_2$, and

R30 $H + O_2 + M \rightarrow HO_2 + M.$

Secondly, except for the first three reactions which involve the metastable oxygen atom, $O(^1D)$, the remaining chemical reactions involve reactants whose formation requires the consumption of an odd hydrogen radical. For example, the formation of nitric acid, HNO_3, takes place only through

the reaction:

R16 $OH + NO_2(+M) \rightarrow HNO_3(+M)$.

Thus, it appears that the actual amount of odd hydrogen radical production in the troposphere is most dependent on the amount of $O(^1D)$ present. In turn, the amount of metastable oxygen atoms in the troposphere is controlled by the photolysis of ozone:

R22 $O_3 + h\nu \rightarrow O_2 + O(^1D)$, $\lambda < 330$ nm.

To determine the production of metastable oxygen atoms, the following must be known:

1. ozone concentration,
2. absorption cross section data of O_3,
3. quantum yield data between 300 and 320 nm, and
4. integrated ozone column density.

A detailed examination of these quantities will be presented later in this report.

Loss of odd hydrogen radicals in the troposphere occurs by the reactions:

R21 $CH_3OOH + OH \rightarrow CH_3O_2 + H_2O$,

R32 $OH + OH \rightarrow H_2O + O$,

R19 $HNO_3 + OH \rightarrow NO_3 + H_2O$,

R18 $CH_4 + OH \rightarrow CH_3 + H_2O$,

R17 $OH + HO_2 \rightarrow H_2O + O_2$,

R20 $HO_2 + HO_2 \rightarrow H_2O_2 + O_2$,

R20a $HO_2 + CH_3O_2 \rightarrow CH_3OOH + O_2$, and

R16 $OH + NO_2(+M) \rightarrow HNO_3(+M)$.

Of the above reactions, only R32 and R17 yield products which cannot readily reform odd hydrogen radicals and the loss of radicals due to the

latter reaction is two to three orders of magnitude greater than the loss created by R32 in the troposphere. For this reason, R32 can be excluded from the reaction sequence without altering the results. This is not to say, however, that the other reactions are not important in the determination of OH abundance. An example of this is the recycling of OH through nitric acid formation and photolysis:

R16 $OH + NO_2(+M) \rightarrow HNO_3(+M)$ and

R6 $HNO_3 + h\nu \rightarrow OH + NO_2$.

Near the ground where the HNO_3 photolysis is relatively low, the above cycle acts as a sink for hydroxyl radicals since heterogeneous removal of nitric acid in this region is a more dominant process than photodissociation. However, in the upper troposphere, where the prescribed amount of NO_2 is less, where heterogeneous processes play a less important role, and where the photolysis rate of HNO_3 is increased, this cycle comes much more into balance and the amount of OH returned by nitric acid photodissociation can even exceed the OH sink brought about by HNO_3 formation. A comprehensive discussion of the effects of heterogeneous processes on the odd hydrogen and odd nitrogen distribution in the troposphere is given by Fishman (1977).

Finally, the last set of reactions which goes into the calculation of tropospheric odd hydrogen radicals are the conversion reactions which are important for determining the ratio of hydroxyl to perhydroxyl radicals. The two reactions which convert HO_2 to OH involve nitrogen oxide and ozone:

R14 $HO_2 + NO \rightarrow OH + NO_2$ and

R15 $HO_2 + O_3 \rightarrow OH + 2\ O_2$.

Conversion of OH to HO_2 occurs through:

R9a $OH + CO \rightarrow H + CO_2$

R9b $OH + CO + M \rightarrow CO_2 + H + M$

R11 $OH + O_3 \rightarrow HO_2 + O_2$

R13 $OH + CH_2O \rightarrow CHO + H_2O$

R10 $OH + H_2 \rightarrow H + H_2O$, and

R12 $OH + H_2O_2 \rightarrow HO_2 + H_2O$.

In the mid-latitude, lower troposphere where anthropogenic emissions determine the amount of carbon monoxide and nitrogen oxides in the air, the ratio of the concentrations of these reactants are most important in the determination of the OH to HO_2 ratio.

A schematic representation of the chemical processes affecting tropospheric odd hydrogen radicals is shown in Figure 1. The rate constants governing these reactions are summarized in Table 1.

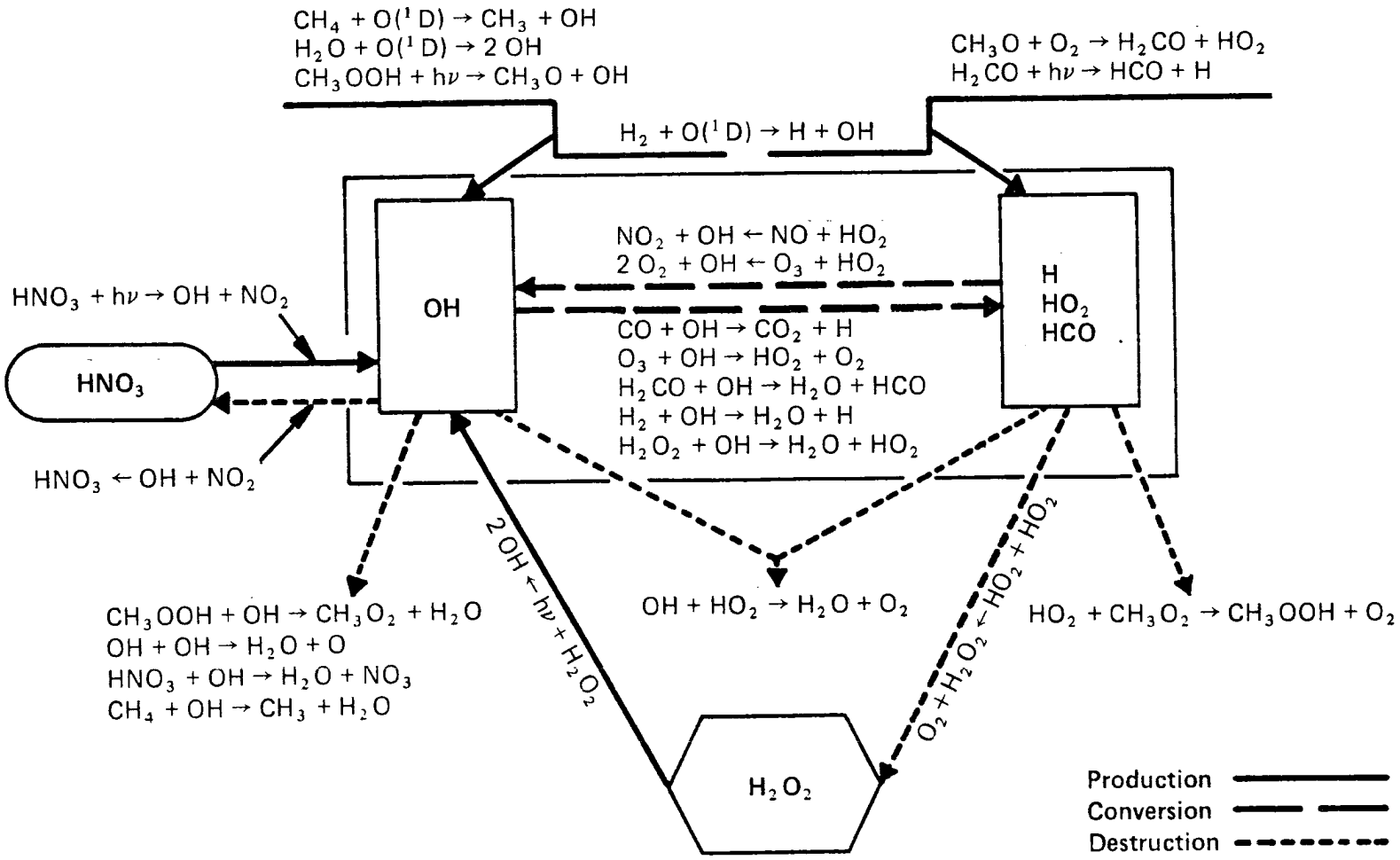

Fig. 1. A schematic diagram of the odd hydrogen photochemistry illustrating the production, destruction, and conversion reactions involving the odd hydrogen radicals (from Fishman, 1977).

TABLE 1

Reactions and Rate Constants

	Reaction	Rate constant	Reference
R1	$H_2O + O(^1D) \rightarrow 2\ OH$	2.3(-10)	NASA (1977)
R2	$H_2 + O(^1D) \rightarrow H + OH$	9.9(-11)	NASA (1977)
R3	$CH_4 + O(^1D) \rightarrow CH_3 + OH$	1.3(-10)	NASA (1977)
R4	$H_2O_2 + h\nu \rightarrow 2\ OH$	j_4	Molina et al. (1977)
R5	$CH_3OOH + h\nu \rightarrow CH_3O + OH$	$j_5 = j_4$ (assumed)	
R6	$HNO_3 + h\nu \rightarrow NO_2 + OH$	j_6	Johnston and Graham (1973)
R7a	$CH_2O + h\nu \rightarrow CHO + H$	3.7(-5)	Calvert et al. (1972)
R7b	$CH_2O + h\nu \rightarrow H_2 + CO$	1.1(-4)	Calvert et al. (1972)
R8	$CH_3O + O_2 \rightarrow CH_2O + HO_2$	1.6(-13) exp (-3300/T)	NASA (1977)
R9a	$CO + OH \rightarrow CO_2 + H$	1.4(-13)	Hampson and Garvin (1975)
R9b	$CO + OH + M \rightarrow CO_2 + H + M$	7.3(-33)	Chan et al. (1977)
R10	$H_2 + OH \rightarrow H_2O + H$	1.8(-11) exp (-2330/T)	Hampson and Garvin (1975)
R11	$O_3 + OH \rightarrow O_2 + HO_2$	1.5(-12) exp (-1000/T)	NASA (1977)
R12	$H_2O_2 + OH \rightarrow H_2O + HO_2$	1.0(-11) exp (-750/T)	NASA (1977)
R13	$CH_2O + OH \rightarrow H_2O + CHO$	3.0(-11) exp (-250/T)	NASA (1977)
R14	$NO + HO_2 \rightarrow NO_2 + OH$	8.0(-12)	Howard and Evenson (1977)
R15	$O_3 + HO_2 \rightarrow 2\ O_2 + OH$	1.0(-13) exp (-1525/T)	NASA (1977)
R16	$NO_2 + OH(+M) \rightarrow HNO_3(+M)$		NASA (1977)
R17	$HO_2 + OH \rightarrow H_2O + O_2$	5.1(-11)	Burrows et al. (1977)

TABLE 1 (cont'd)

	Reaction	Rate constant	Reference
R18	$CH_4 + OH \rightarrow CH_3 + H_2O$	2.4(-12) exp (-1710/T)	NASA (1977)
R19	$HNO_3 + OH \rightarrow NO_3 + H_2O$	8.0(-14)	NASA (1977)
R20	$HO_2 + HO_2 \rightarrow H_2O_2 + O_2$	5.0(-11) exp (-500/T)	NASA (1977)
R20a	$CH_3O_2 + HO_2 \rightarrow CH_3OOH + O_2$	$k_{20a} = k_{20}$	assumed
R21	$CH_3OOH + OH \rightarrow CH_3O_2 + H_2O$	$k_{21} = k_{17}$	assumed
R22	$O_3 + h\nu \rightarrow O_2 + O(^1D)$	See text	
R23	$O(^1D) + M \rightarrow O + M$	5.0(-11)	NASA (1977)
R24	$NO + O_3 \rightarrow NO_2 + O_2$	2.1(-12) exp (-1450/T)	NASA (1977)
R25	$NO_2 + h\nu \rightarrow NO + O$	j_{25}	Hampson and Garvin (1975)
R26a	$H_2O_2 \rightarrow$ heterogeneous removal	2.0(-5) - 2.4(-6) x f(z)	See text
R26b	$CH_3OOH \rightarrow$ heterogeneous removal	2.0(-5) - 2.4(-6) x f(z)	See text
R27	$CH_3CCl_3 + OH \rightarrow H_2O + CH_2CCl_3$	3.5(-12) exp (-1562/T)	NASA (1977)
R28	$O + O_2 + M \rightarrow O_3 + M$	6.6(-35) exp (-510/T)	Hampson and Garvin (1975)
R29	$CH_3 + O_2 + M \rightarrow CH_3O_2 + M$	2.6(-31)	Hampson and Garvin (1975)
R30	$H + O_2 + M \rightarrow HO_2 + M$	6.7(-33) exp (290/T)	Hampson and Garvin (1975)
R31	$CHO + O_2 \rightarrow CO + HO_2$	6.0(-12)	NASA (1977)
R32	$OH + OH \rightarrow H_2O + O$	1.0(-11) exp (-550/T)	NASA (1977)
R33	$CH_3O_2 + NO \rightarrow CH_3O + NO_2$	$k_{33} = k_{14}$	Assumed

TABLE 1 (cont'd)

Table 1. Reactions and reaction rate constants used in this study.

Most rate constants are as recommended for a recent Chlorofluoromethane Assessment Workshop (NASA, 1977).

$f(z) = \exp [-0.46 (k-5)]$, $k >$ kms $= 1.0$, $k \leq 5$ kms.
Numbers in parenthesis indicate to powers of ten.

Units for unimolecular rate constants are s^{-1}; bimolecular are cm^3 $mol.^{-1} s^{-1}$; trimolecular are cm^3 $mol.^{-1}$ s^{-1}.

III. CALCULATION OF ODD HYDROGEN RADICAL NUMBER DENSITIES

Because of the highly reactive nature of these radicals, it is assumed that each of them is in a photo-stationary state. By doing so, the assumption is made that $d[OH]/dt = d[HO_2]/dt = 0$. If we let P be the photochemical production rate of X (where X represents either OH or HO_2) and D the destruction rate of X, the above assumption permits

$$\frac{d[X]}{dt} = P - [X] \cdot D = 0. \tag{1}$$

Furthermore, we couple the individual expressions of (1) for OH and HO_2 which produces the following set of equations:

$$P_1 + P_2[HO_2] - D_1[OH] = 0 \text{ and} \tag{2}$$

$$P_3 + P_4[OH] - D_2[HO_2] - D_3[HO_2]^2 = 0. \tag{3}$$

In the above equations, P_1 is the set of reactions which produce OH without consuming a perhydroxyl radical; P_2 consists of the reactions which convert HO_2 to OH; D_1 is the destruction rate of OH; P_2 and P_4 are the counterparts of P_1 and P_2, but for the HO_2 radical; D_2 and D_3 are the destruction frequencies of HO_2.

For these particular calculations, the following relations are defined for the various terms in Eqs. (2) and (3):

$$P_1 = [O(^1D)] \cdot \{2 \cdot [H_2O] \cdot k_1 + [H_2] \cdot k_2 + [CH_4] \cdot k_3\} + 2 \cdot [H_2O_2] \cdot j_4 + [CH_3OOH] \cdot j_5 + [HNO_3] \cdot j_6$$

$$P_2 = [NO] \cdot k_{14} + [O_3] \cdot k_{15}$$

$$D_1 = [HO_2] \cdot k_{17} + [NO_2] \cdot k_{16} + [CH_3OOH] \cdot k_{21}$$
$$+ [CH_4] \cdot k_{18} + [HNO_3] \cdot k_{19} + [CO] \cdot \{k_{9a} + [M]\, k_{9b}\}$$
$$+ [O_3] \cdot k_{11} + [CH_2O] \cdot k_{13} + [H_2] \cdot k_{10} + [H_2O_2] \cdot k_{12}$$

$$P_3 = [H_2] \cdot [O(^1D)] \cdot k_2 + [CH_3O] \cdot [O_2] \cdot k_8 + 2 \cdot [CH_2O] \cdot j_{7a}$$

$$P_4 = [CO] \cdot \{k_{9a} + [M] \cdot k_{9b}\} + [O_3] \cdot k_{11} + [H_2] \cdot k_{10}$$
$$+ [H_2O_2] \cdot k_{12}$$

$$D_2 = [NO] \cdot k_{14} + [O_3] \cdot k_{15} + [CH_3O_2] \cdot k_{20a} + [OH] \cdot k_{17}$$

$$D_3 = 2 \cdot k_{20}.$$

The expression for [OH] in Equation (2):

$$[OH] = \frac{P_2 + P_2[HO_2]}{D_1} \tag{2a}$$

can be substituted into Equation (3) giving:

$$-\left(P_3 + \frac{P_4 P_1}{D_1} + \left(D_2 - \frac{P_4 P_2}{D_1}\right)[HO_2] + D_3[HO_2]^2 = 0\right. \tag{3a}$$

where $[HO_2]$ can be solved directly using the standard quadratic formula. Once $[HO_2]$ is computed explicitly, [OH] is readily found from Eq (2a). Solutions to Eqs. (2a) and (3a) are iterated five times which produces differences between successive iterations comparable to the accuracy of the computer.

IV. INPUT DATA

To compute the global distribution of odd hydrogen radicals, input distributions of several trace constituents must be known; these gases include:

1. ozone,
2. water vapor,
3. carbon monoxide, and
4. nitrogen oxides.

The distribution of tropospheric ozone and water vapor are important since the amount of each of these species determines the amount of initial production of radicals through the sequence of reactions

R22 $O_3 + h\nu \rightarrow O(^1D) + O_2$, $\lambda < 320$ nm

and R1 $O(^1D) + H_2O \rightarrow 2\ OH$.

The amount of CO and NO are important since the relative concentrations of these gases determine the OH to HO_2 ratio through the conversion reactions:

R9a(b) $OH + CO(+M) \rightarrow CO_2 + H(+M)$

(R30 $H + O_2 + M \rightarrow HO_2 + M$)

and R14 $HO_2 + NO \rightarrow OH + NO_2$.

Unfortunately, only the global distribution of CO had been published in the literature (Seiler, 1974) before this research was initiated. Data for tropospheric ozone in the Northern Hemisphere were available from Chatfield and Harrison (1977b) and Northern Hemisphere water vapor content was given in U.S. Standard Atmosphere Supplement (1966). The latter set of data did not yield enough temporal resolution and was revised in later calculations using the climatological data available at the National Center for Atmospheric Research. At present, a good

representation of tropospheric NO_x still does not exist. A complete description of the input data used for the model calculations is given in the following sections.

Until recently, a good description of the distribution of tropospheric ozone with respect to latitude, altitude, and season had not been published. Although no specific observational program was ever established to make such a data set available, the efforts of Chatfield and Harrison (1977a, 1977b) produced a comprehensive analysis of existing ozonesonde data taken by the North American Ozonesonde Network (primarily in the 1960's). Thus, we have used the data given in Chatfield and Harrison (1977b) as our input for the calculations described previously.

Because a comprehensive analysis of tropospheric ozone in the Southern Hemisphere was not available prior to this study, substantial effort was devoted to compiling such a data set. The primary sources for these data were Ozone Data for the World, a bimonthly publication of the Canadian Department of Transportation dating back to 1962 and an analysis of ozonesonde data from Aspendale by Pittock (1974). Whereas the Aspendale data consisted of over 400 ozonesondes, only about 170 soundings were available from other sites in the Southern Hemisphere. This fact indicates that the data to be presented may not be as representative of true seasonal and latitudinal averages as one would desire. Nevertheless, we contend that this data is probably the most comprehensive that exists and that the situation cannot be improved until a comprehensive sampling program in the Southern Hemisphere is developed.

Ozone Data for the World gives five Southern Hemisphere sites which have launched ozonesondes in the 1960's and 1970's in addition to

occasional soundings available from ships. The data analyzed in this study primarily consisted of soundings taken from the following stations: Canton Island (3°S), La Paz (16°S), Aspendale (38°S), Christchurch (43°S), and Syowa (69°S). The Aspendale data previously had been analyzed by Pittock (1974) and his monthly and altitude distribution has been used as part of our analysis of the entire Southern Hemisphere. Because of the sparse nature of the data available from the remaining stations, all soundings were classified into three-month (seasonal) groups to minimize the effects of any one anomalous profile.

The meridional distribution of ozone averaged over the entire year is depicted in Fig. 2. The tropospheric ozone distributions representative of the months of January and July are presented in Figs. 3a and 3b, respectively. Note that the units of these analyses are expressed in volume mixing ratio concentrations and that volume mixing ratios greater than 100 parts per billion (ppbv) are assumed to be stratospheric air.

Figure 4a is presented to show the summer-winter ozone profile difference in the mid-latitudes for the Northern Hemisphere. Of primary importance is the fact that 20 to 30% more ozone is present below seven kilometers in the summer even though stratospheric-tropospheric exchange processes are more prevalent in the winter (e.g., see Danielsen, 1968). This suggests that more photochemical production of ozone in the lower troposphere may take place at these latitudes in the summer. Although a similar phenomenon takes place at 15°N, it is not as clearly seen at 5°N (Fig. 4b). The reason for this phenomenon is difficult to assess without looking at both the

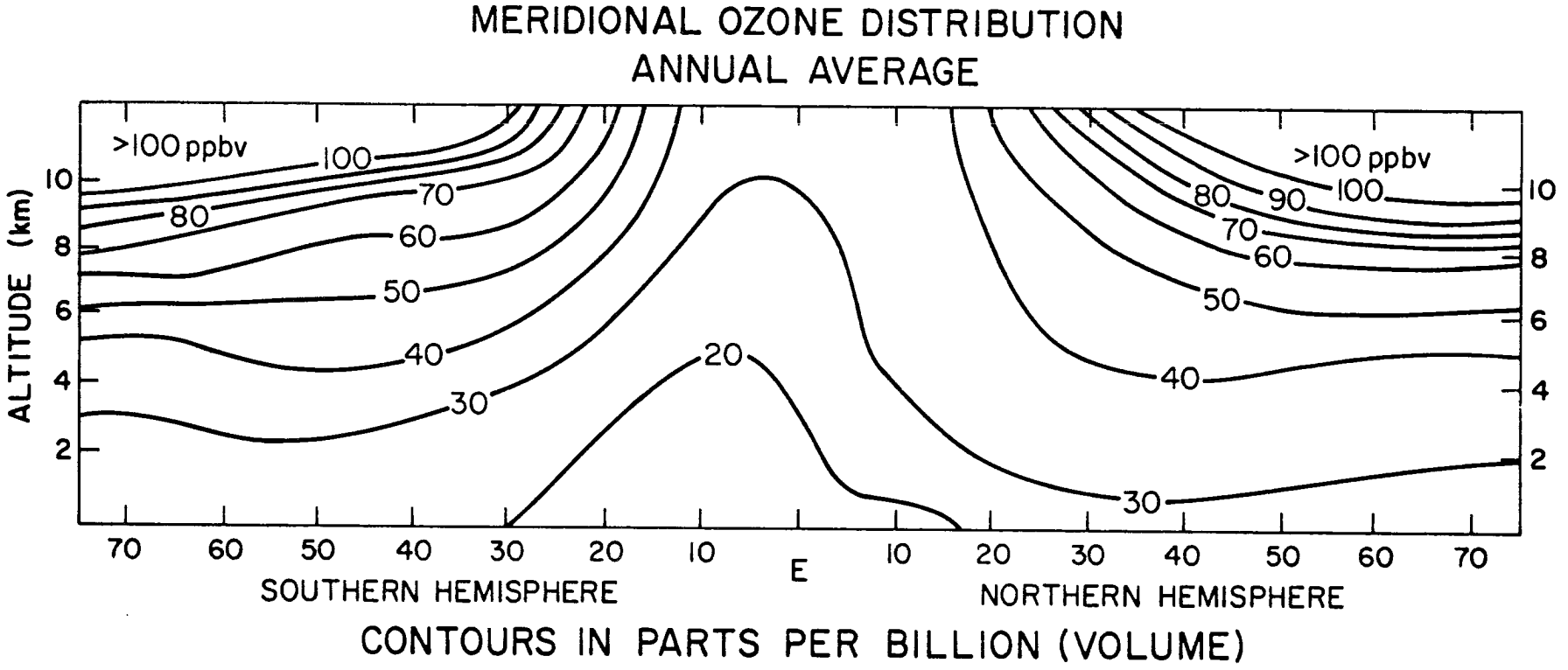
MERIDIONAL OZONE DISTRIBUTION
ANNUAL AVERAGE
>100 ppbv
100
80
70
60
50
40
30
20
>100 ppbv
100
90
80
70
60
50
40
30
ALTITUDE (km)
10
8
6
4
2
70 60 50 40 30 20 10
E
10 20 30 40 50 60 70
SOUTHERN HEMISPHERE
NORTHERN HEMISPHERE
CONTOURS IN PARTS PER BILLION (VOLUME)

Fig. 2

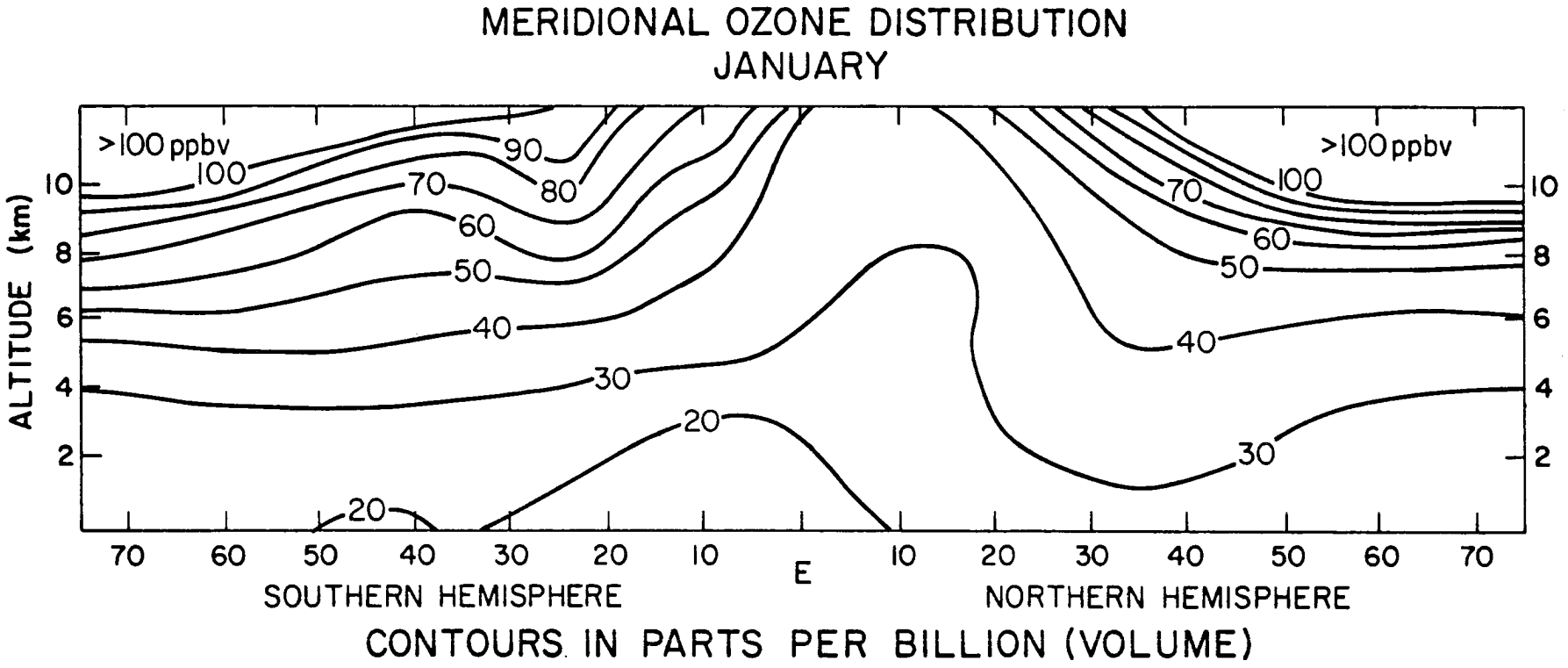
MERIDIONAL OZONE DISTRIBUTION
JANUARY
ALTITUDE (km)
>100 ppbv
100
90
80
70
60
50
40
30
20
>100 ppbv
100
70
60
50
40
30
20
10
8
6
4
2
70 60 50 40 30 20 10 E 10 20 30 40 50 60 70
SOUTHERN HEMISPHERE
NORTHERN HEMISPHERE
CONTOURS IN PARTS PER BILLION (VOLUME)

Fig. 3a

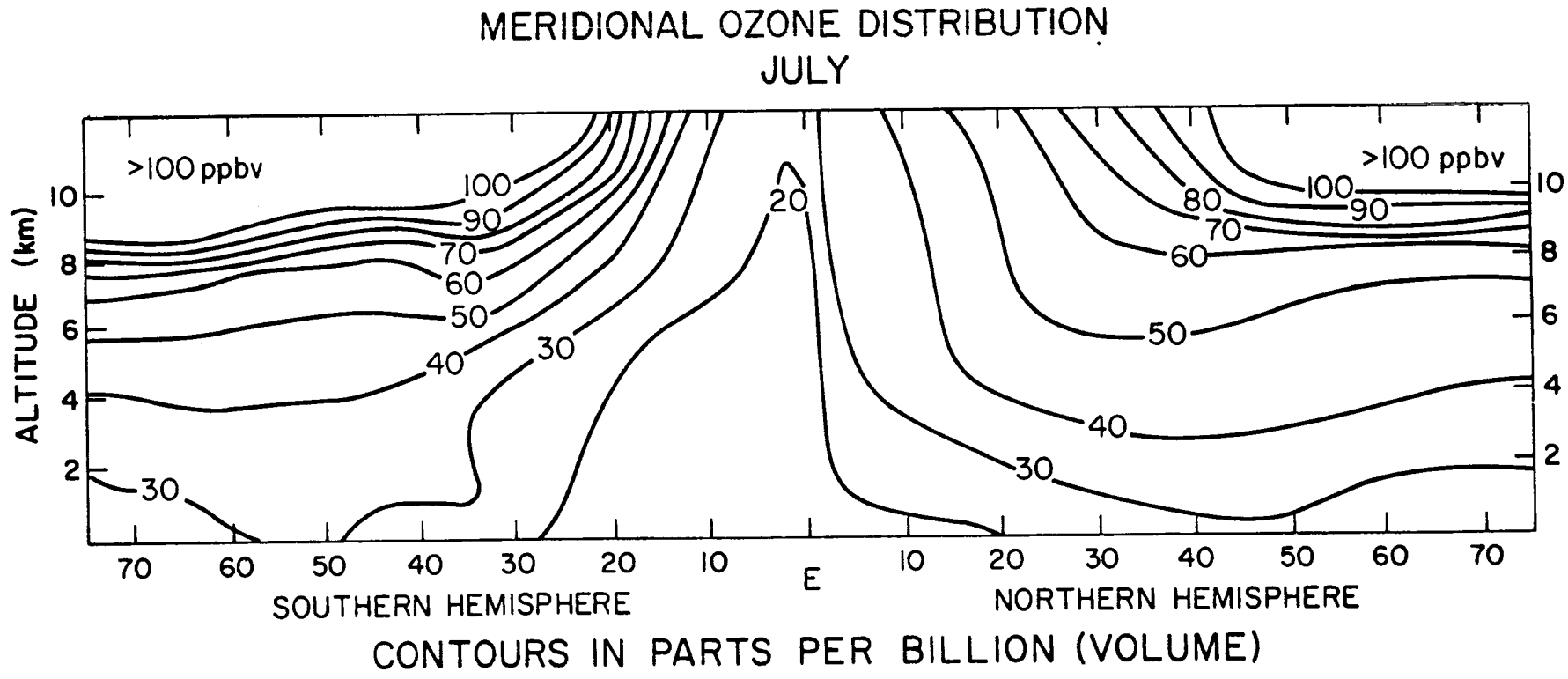
MERIDIONAL OZONE DISTRIBUTION
JULY
>100 ppbv
>100 ppbv
100
90
80
70
60
50
40
30
20
ALTITUDE (km)
10
8
6
4
2
70
60
50
40
30
20
10
E
10
20
30
40
50
60
70
SOUTHERN HEMISPHERE
NORTHERN HEMISPHERE
CONTOURS IN PARTS PER BILLION (VOLUME)

Fig. 3b

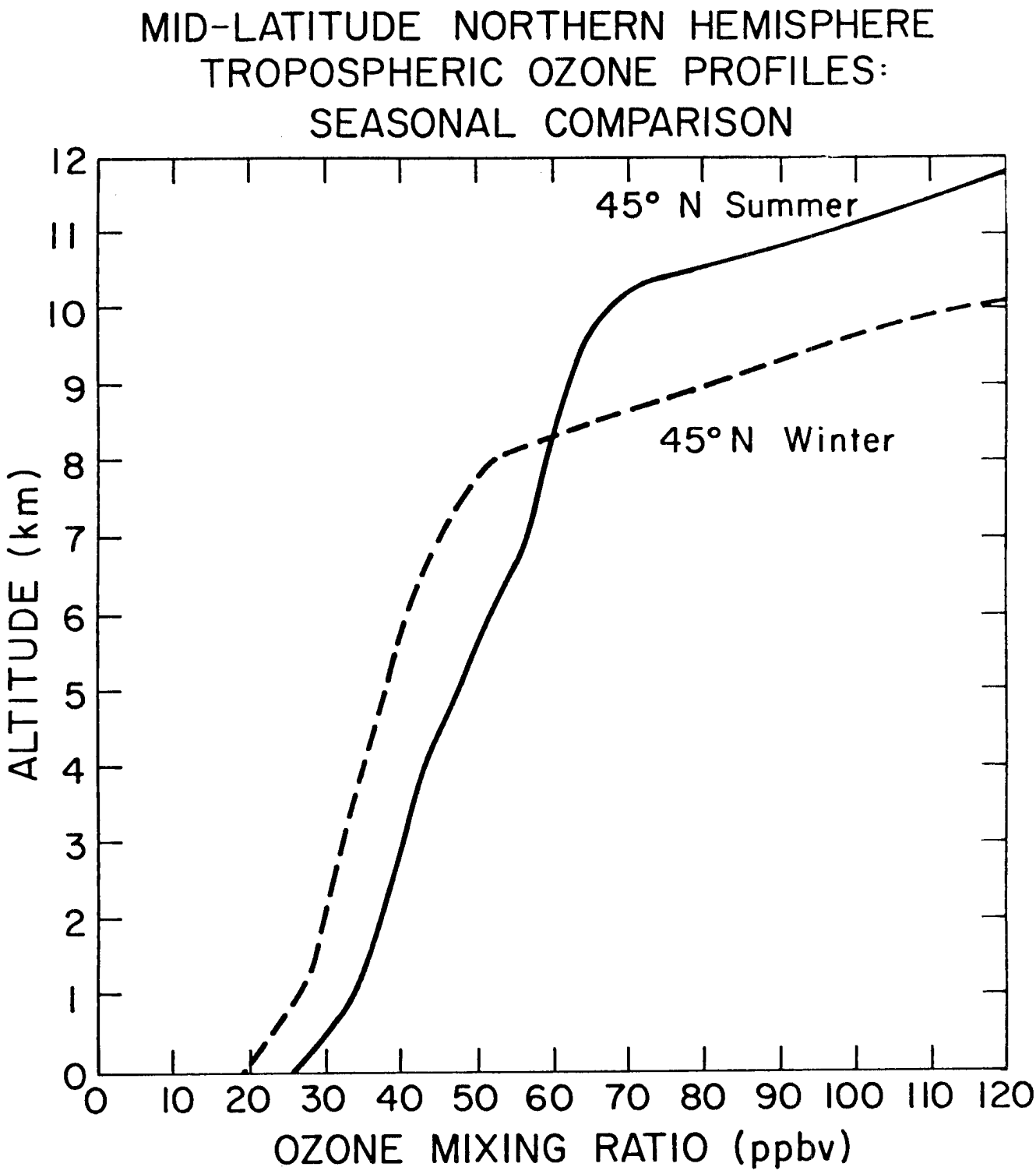
MID-LATITUDE NORTHERN HEMISPHERE
TROPOSPHERIC OZONE PROFILES:
SEASONAL COMPARISON
45° N Summer
45° N Winter
ALTITUDE (km)
0
1
2
3
4
5
6
7
8
9
10
11
12
0
10
20
30
40
50
60
70
80
90
100
110
120
OZONE MIXING RATIO (ppbv)

Fig. 4a

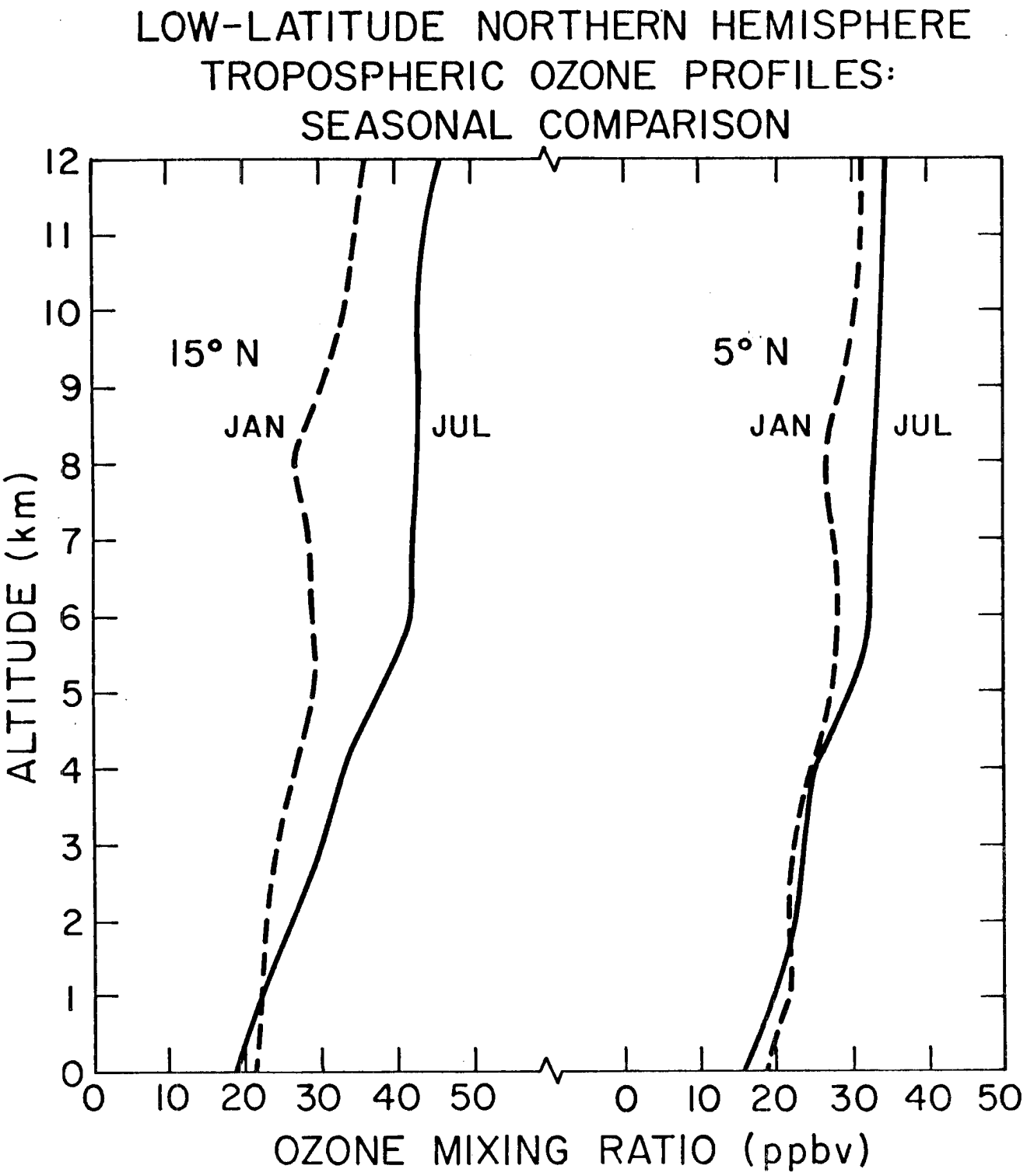
LOW-LATITUDE NORTHERN HEMISPHERE
TROPOSPHERIC OZONE PROFILES:
SEASONAL COMPARISON
15° N
JAN
JUL
5° N
JAN
JUL
ALTITUDE (km)
0
1
2
3
4
5
6
7
8
9
10
11
12
0 10 20 30 40 50
0 10 20 30 40 50
OZONE MIXING RATIO (ppbv)

Fig. 4b

meteorological dynamics and photochemistry in much detail. The analysis of the tropospheric ozone budget presented in Section V does support the hypothesis that ozone may be produced photochemically in Northern Hemisphere mid-latitudes (Fishman and Crutzen, 1977) and transported to lower latitudes, but one must examine troposphere-stratosphere exchange properties as a function of both season and latitude to determine what effect this mechanism would have on the data shown in Figs 3a and 3b. Future research efforts will be devoted to obtaining a better picture of the meteorological dynamics in order to resolve what tropospheric ozone distribution one might expect considering stratosphere-troposphere exchange processes only.

The seasonal variation in the Southern Hemisphere mid-latitudes (40^{o}S) is shown in Fig. 5. Unlike the variation in the Northern Hemisphere mid-latitudes (Fig. 4a), more ozone is observed in the winter than in the summer at this latitude which suggests that mixing may play the predominant role in determining the tropospheric ozone distribution in all seasons. If photochemical production were the dominant source of ozone in this region, one might expect more tropospheric ozone in the summer when this mechanism is enhanced. However, the meteorological dynamics of the Southern Hemisphere must be examined in detail in future research to determine if this seasonal variation of tropospheric ozone is consistent with large scale transport processes in this hemisphere. Another feature of these profiles is that the total seasonal variation in the Southern Hemisphere mid-latitudes is less than in the Northern Hemisphere. This point has previously been brought forth by Pittock (1974) who compared his data with Dütsch (1970).

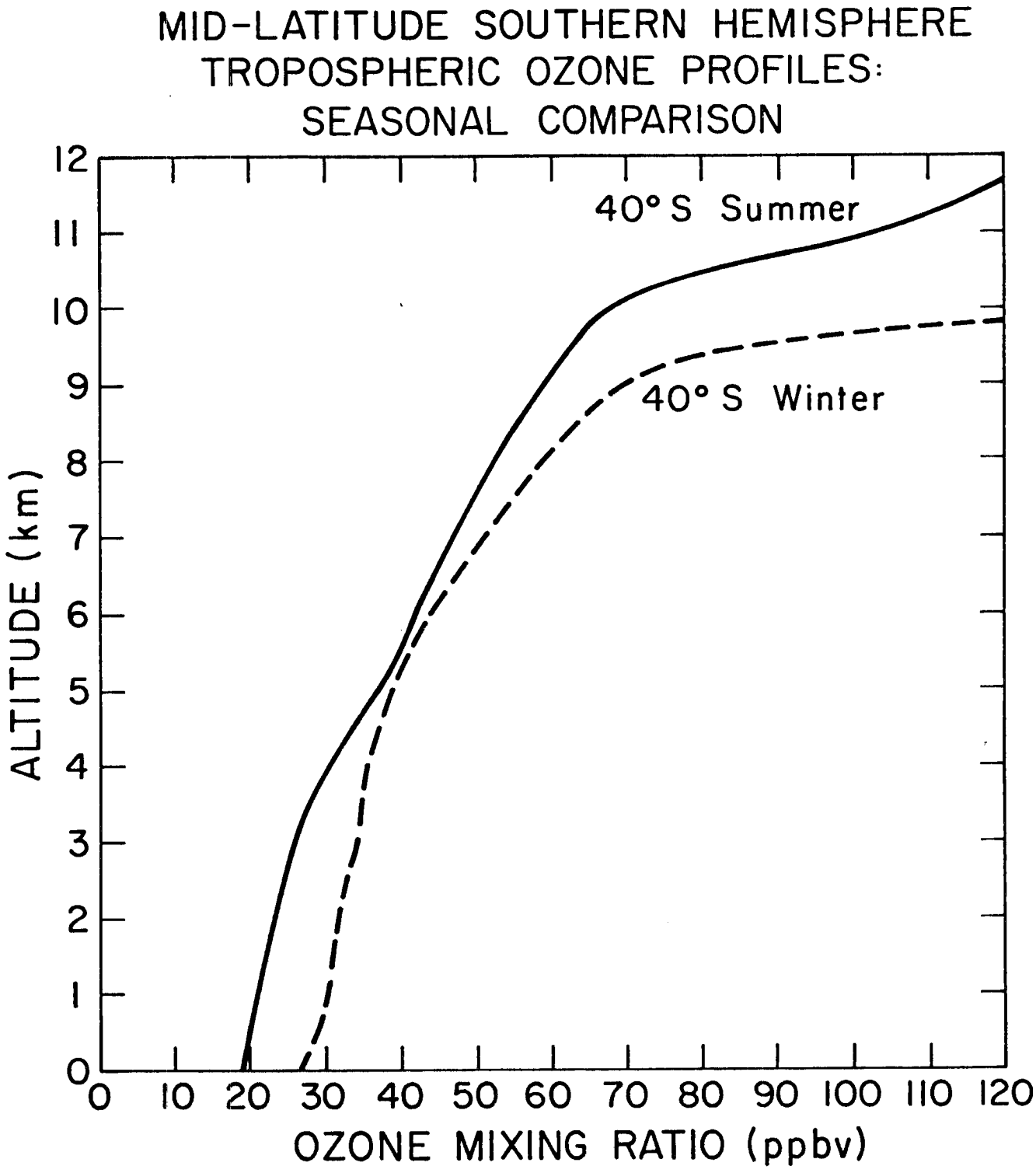
MID-LATITUDE SOUTHERN HEMISPHERE
TROPOSPHERIC OZONE PROFILES:
SEASONAL COMPARISON
40° S Summer
40° S Winter
ALTITUDE (km)
0
1
2
3
4
5
6
7
8
9
10
11
12
0
10
20
30
40
50
60
70
80
90
100
110
120
OZONE MIXING RATIO (ppbv)

Fig. 5

Figure 6 depicts the interhemispheric difference in the mid-latitude tropospheric ozone profiles for respective summer seasons. Particularly noteworthy in this comparison is the fact that ozone concentrations and the shapes of these profiles above 10 kms are nearly identical. On the other hand, the Northern Hemisphere average summer ozone concentrations are 15 to 20 ppb greater (30-70%) than the corresponding concentrations in the Southern Hemisphere between one and eight kms.

Figure 7 shows that when the ozone data are averaged over the entire year, we observe more ozone in the Northern Hemisphere troposphere at low latitudes. At 5^{o}, Northern Hemisphere concentrations are 7 to 13 ppb greater (30-100%) between 1 and 8 kms whereas the profiles converge at 12 kms. Similarly, at 15^{o}, we find 5 to 12 ppb more (20-65%) ozone in the Northern Hemisphere mid-troposphere even though there are slightly higher concentrations in the Southern Hemisphere above 10 kms.

Lastly, we point out that the similarity of ozone concentrations in the upper troposphere at all corresponding latitudes of the two hemispheres makes the differences observed between the low and middle troposphere of the two hemispheres more credible. If these hemispheric differences are real (and not merely the product of inadequate data or faulty analysis), they suggest that there are important differences in the photochemical and/or physical processes taking place in these hemispheres. These points will be discussed in the next section.

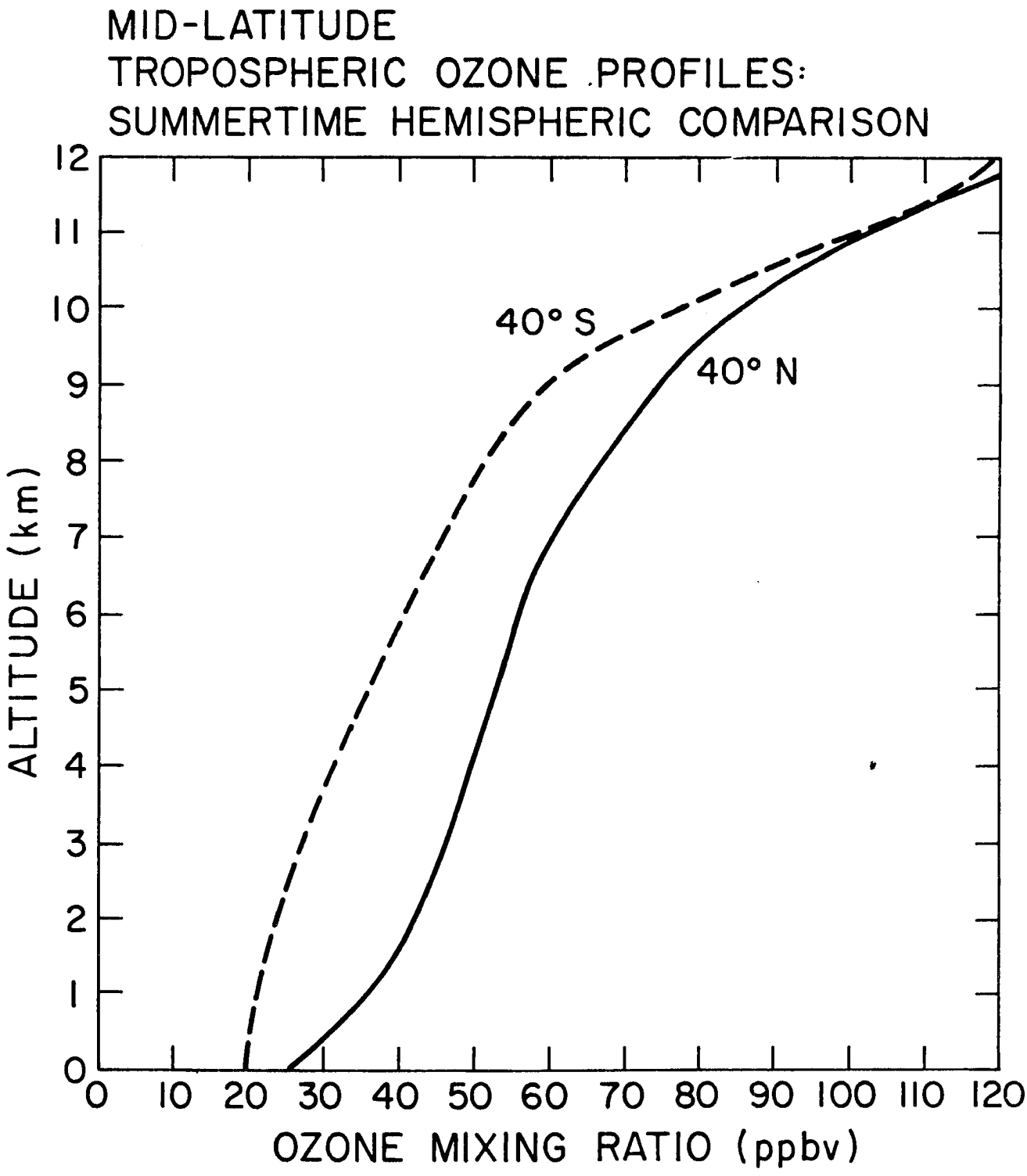
MID-LATITUDE
TROPOSPHERIC OZONE PROFILES:
SUMMERTIME HEMISPHERIC COMPARISON
40° S
40° N
ALTITUDE (km)
0
1
2
3
4
5
6
7
8
9
10
11
12
0
10
20
30
40
50
60
70
80
90
100
110
120
OZONE MIXING RATIO (ppbv)

Fig. 6

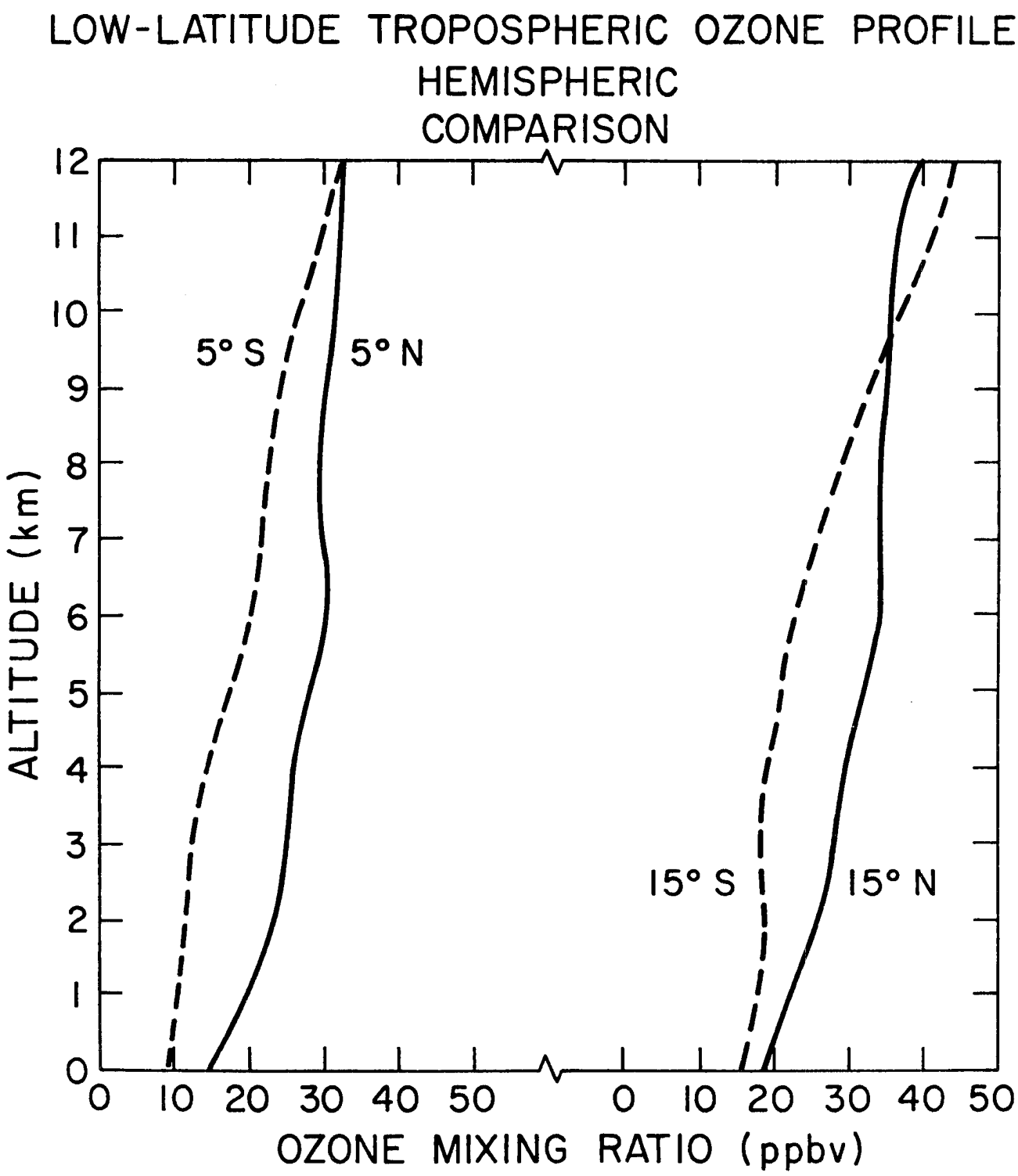
LOW-LATITUDE TROPOSPHERIC OZONE PROFILES:
HEMISPHERIC
COMPARISON
5° S
5° N
15° S
15° N
ALTITUDE (km)
0
1
2
3
4
5
6
7
8
9
10
11
12
0
10
20
30
40
50
0
10
20
30
40
50
OZONE MIXING RATIO (ppbv)

Fig. 7

V. TROPOSPHERIC OH AND AN EXAMINATION OF THE EFFECTS OF CERTAIN MODEL PARAMETERS ON ITS DISTRIBUTION

Whereas the amount of ozone is directly responsible for determining the amount of odd hydrogen radicals produced in the troposphere, we recall that the relative amounts of carbon monoxide and nitrogen oxides (NO_x) primarily determine the ratio of OH to HO_2 through the reactions:

R9a(b) $OH + CO(+M) \rightarrow H + CO_2(+M)$,

(R30 $H + O_2 + M \rightarrow HO_2 + M$), and

R14 $HO_2 + NO \rightarrow OH + NO_2$.

The most comprehensive analysis of CO has been carried out by Seiler (1974); his data are used as input for the current study. Figure 8 depicts four tropospheric CO profiles representative of mid- and low latitudes in both hemispheres. Particularly noteworthy is the uniform decrease in surface and low altitude CO concentrations as one progresses southward. At low altitudes, the amount of CO at 45^{o}N is more than three times larger than the concentration at 45^{o}S; this factor decreases to two in the middle troposphere whereas equal concentrations are found at the mid-latitude tropopause height (12 km) in the two hemispheres.

At 15^{o}, we note that there is 70% more CO near the surface in the Northern Hemisphere than in the Southern Hemisphere but that at 6 kms, less than a 10% difference is observed. Recalling that the hemispheric difference of ozone at these latitudes is 20-65% at these altitudes, one could estimate that the calculated amount of OH at these two latitudes would be quite comparable; this speculation is borne out by the calculated tropospheric average concentrations: 5.1×10^{5} cm^{-3}

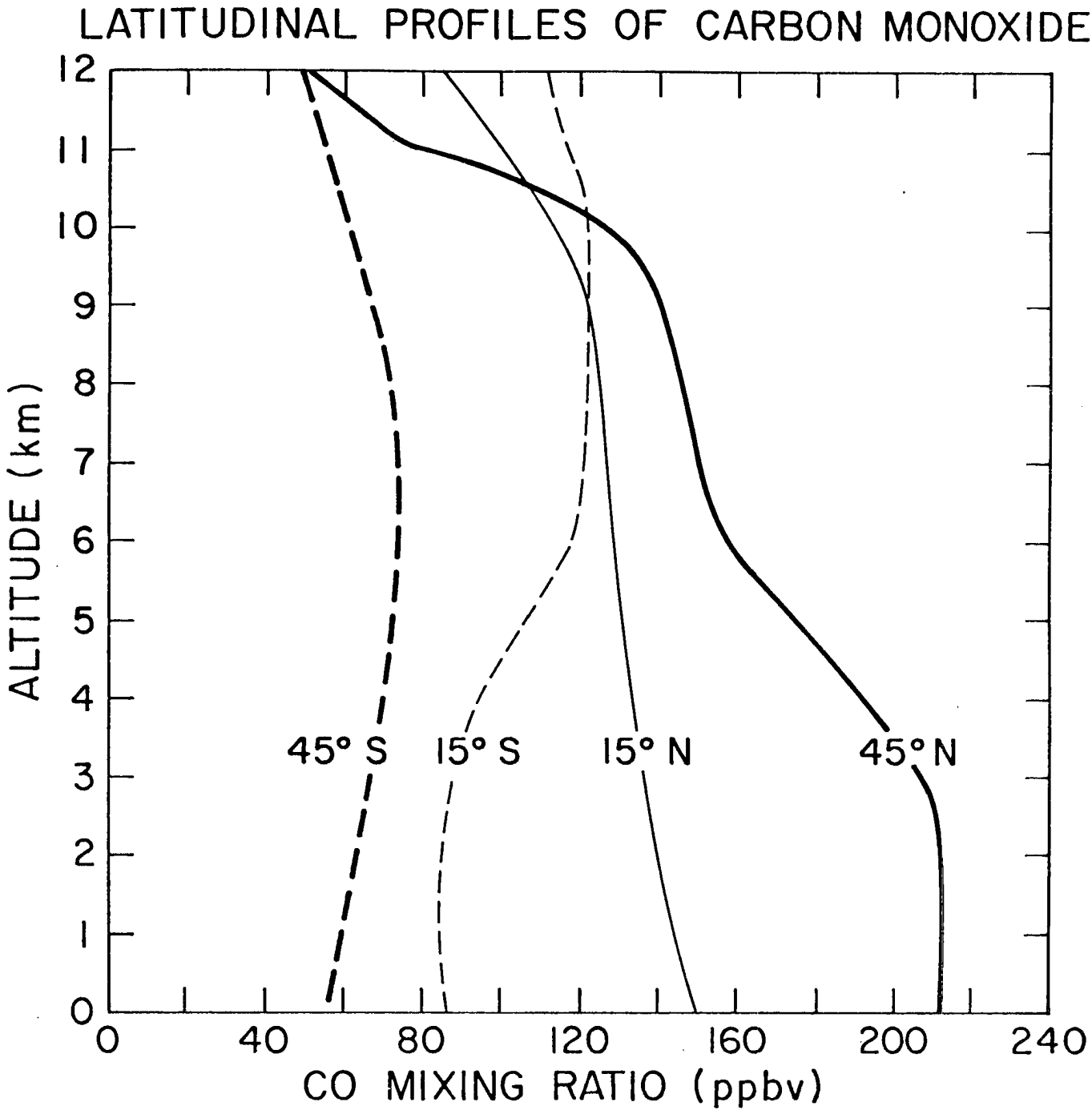

Fig. 8. (Seiler, 1974)

at 15^{o}N vs. 4.5×10^{5} cm^{-3} at 15^{o}S. Using the fact that there is more OH at 15^{o}N than at 15^{o}S, one would expect a greater difference in OH at 5^{o}N and 5^{o}S since the CO differences are smaller (0-25%) and the ozone differences are larger (30-100%) than at 15^{o}. The calculations indicate a 40% difference: 5.8×10^{5} cm^{-3} at 5^{o}N and 4.1×10^{5} cm^{-3} at 5^{o}S. [Note that for all the latitudes discussed above (and for all latitudes 15^{o}N and southward), the concentration of NO_x at every latitude is the same for any corresponding altitude.]

The above analysis is presented to show why we should not be surprised by the fact that there is slightly more OH in the Northern Hemisphere (3.3×10^{5} cm^{-3}) than in the Southern Hemisphere troposphere (2.9×10^{5} cm^{-3}). This finding is contrary to the analysis of Crutzen and Fishman (1977) who hypothesized that the average OH concentration should be 2.7 times larger in the Southern Hemisphere because of less CO in this hemisphere, and Singh (1977b) who analyzed the tropospheric distribution of methyl chloroform to suggest that this ratio be between 1.6 and 3.0. The primary reason for the discrepancy noted here can be directly attributed to the difference in the amount of tropospheric ozone in the two hemispheres.

Figure 9 shows the diurnally and monthly averaged OH distribution in the troposphere. Although the highest average OH concentration is found in the Southern Hemisphere (15^{o}S at the surface), a much stronger intrahemispheric gradient exists both latitudinally and vertically resulting in comparable amounts of OH in both hemispheres. To see how the computed OH distributions vary seasonably, Figs. 10a, b, c, and d are presented. As expected, more OH is computed for each respective hemisphere's summer season (about three times higher than

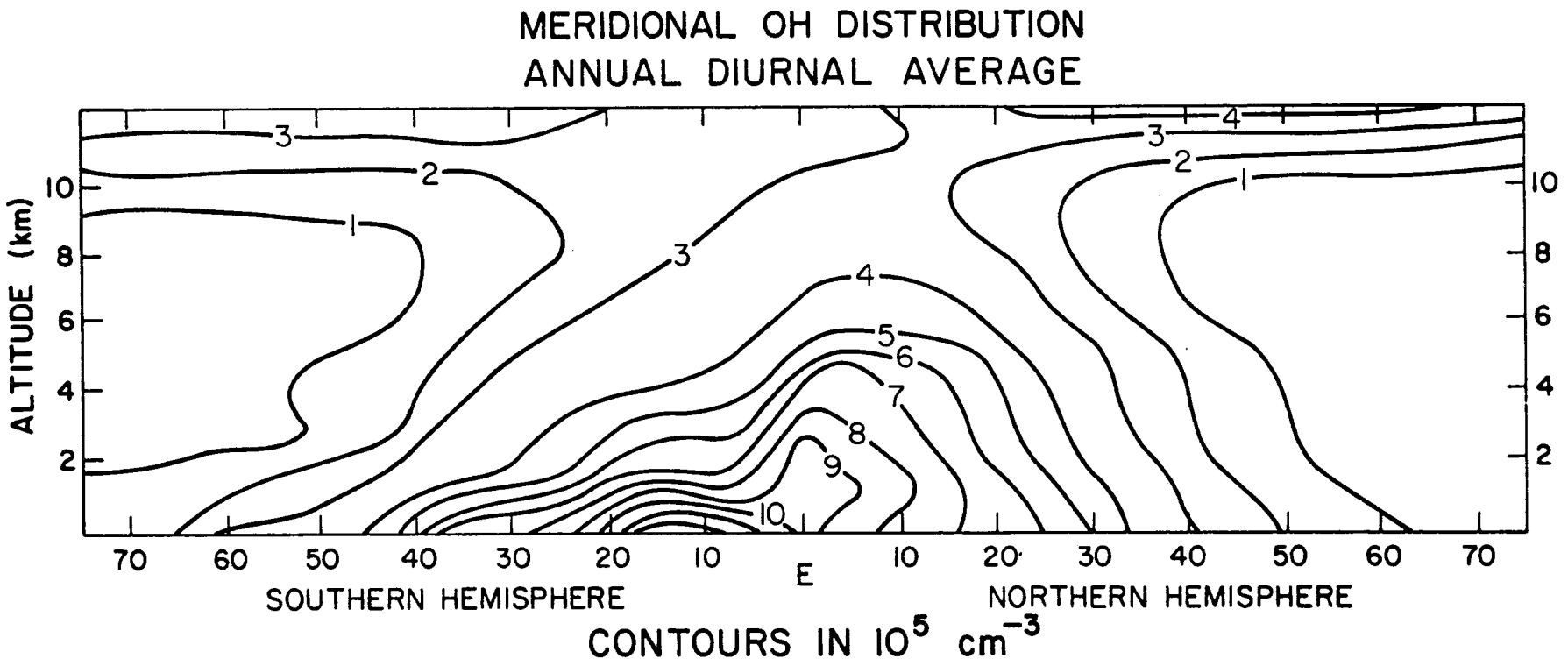
MERIDIONAL OH DISTRIBUTION
ANNUAL DIURNAL AVERAGE
ALTITUDE (km)
10
8
6
4
2
1
2
3
4
5
6
7
8
9
10
70 60 50 40 30 20 10 E 10 20 30 40 50 60 70
SOUTHERN HEMISPHERE
NORTHERN HEMISPHERE
CONTOURS IN 10^5 cm^{-3}

Fig. 9

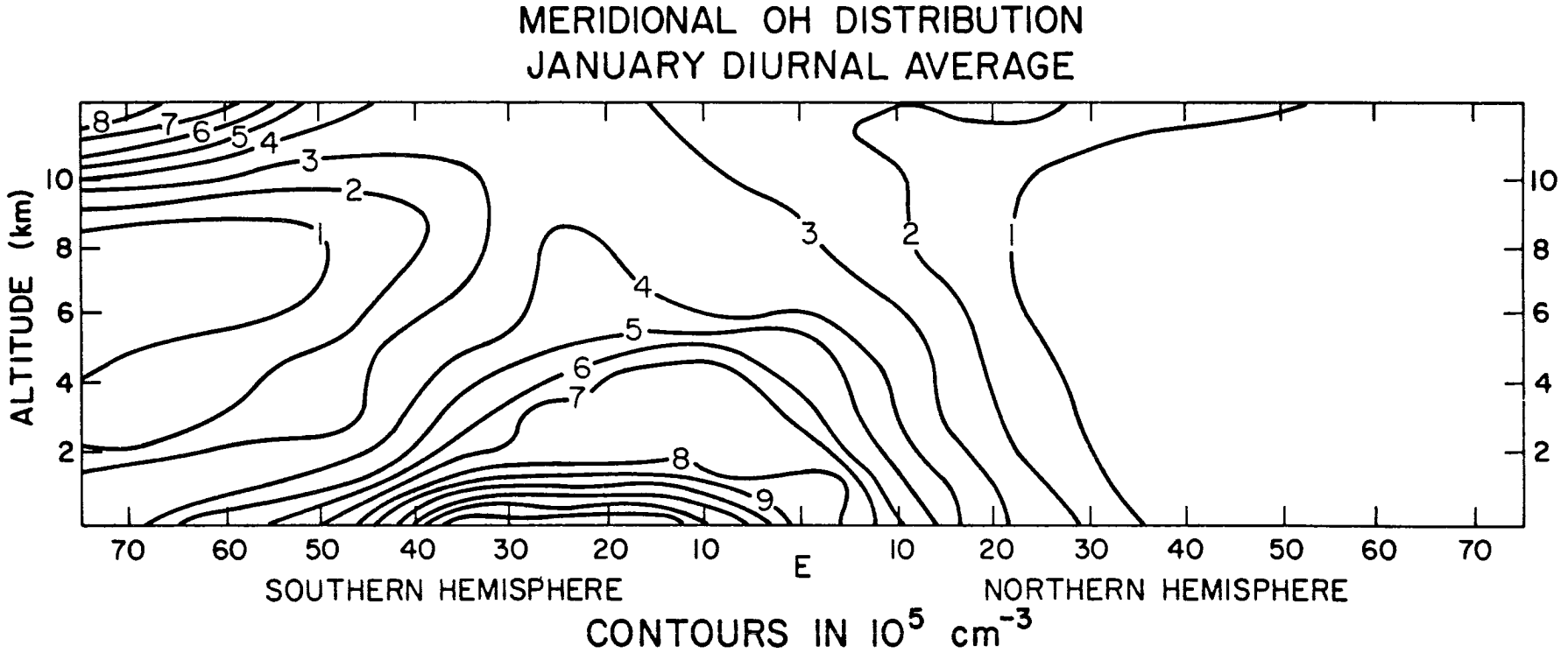
MERIDIONAL OH DISTRIBUTION
JANUARY DIURNAL AVERAGE
ALTITUDE (km)
10
8
6
4
2
1
2
3
4
5
6
7
8
9
70 60 50 40 30 20 10 E 10 20 30 40 50 60 70
SOUTHERN HEMISPHERE
NORTHERN HEMISPHERE
CONTOURS IN 10^5 cm^{-3}

Fig. 10a

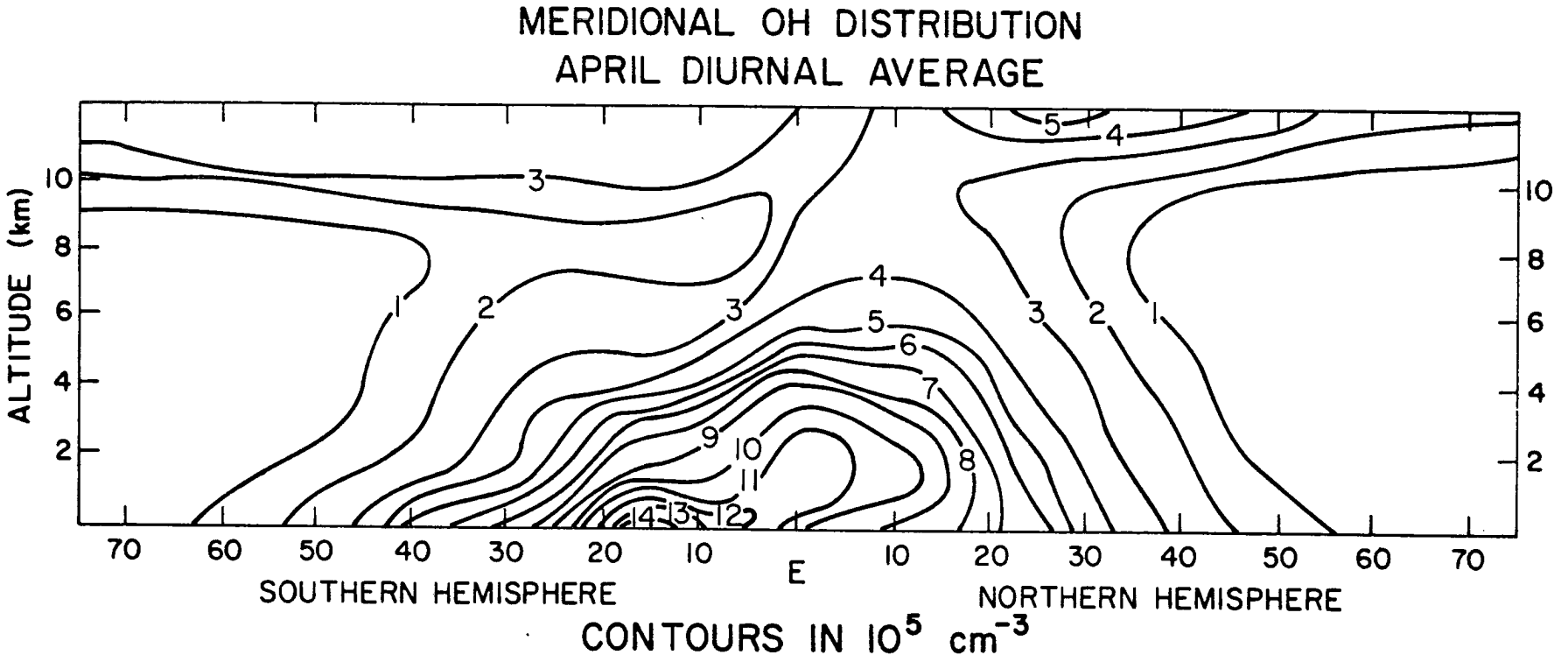
MERIDIONAL OH DISTRIBUTION
APRIL DIURNAL AVERAGE
ALTITUDE (km)
10
8
6
4
2
70
60
50
40
30
20
10
E
10
20
30
40
50
60
70
SOUTHERN HEMISPHERE
NORTHERN HEMISPHERE
CONTOURS IN 10^5 cm^{-3}

Fig. 10b

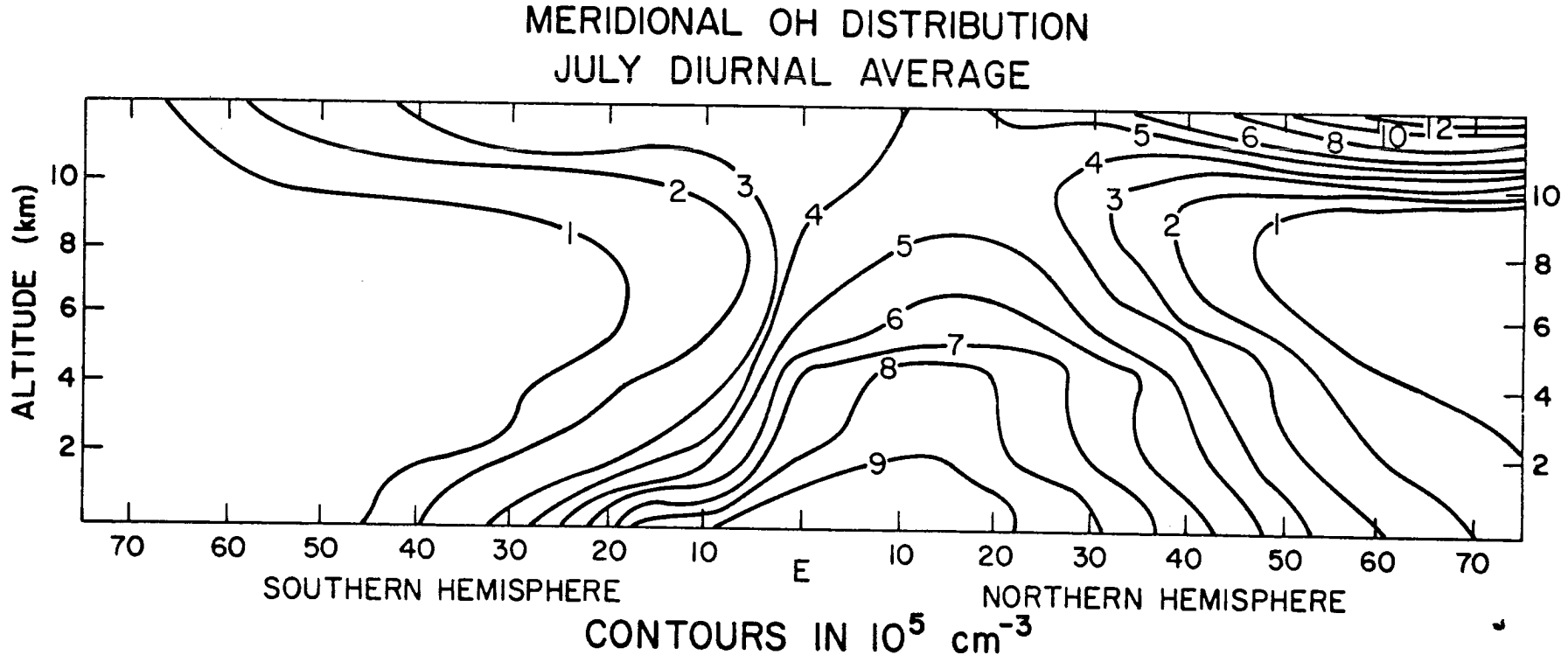
MERIDIONAL OH DISTRIBUTION
JULY DIURNAL AVERAGE
ALTITUDE (km)
10
8
6
4
2
1
2
3
4
5
6
7
8
9
5
6
8
10
12
4
3
2
1
70 60 50 40 30 20 10 E 10 20 30 40 50 60 70
SOUTHERN HEMISPHERE
NORTHERN HEMISPHERE
CONTOURS IN 10^5 cm^{-3}

Fig. 10c

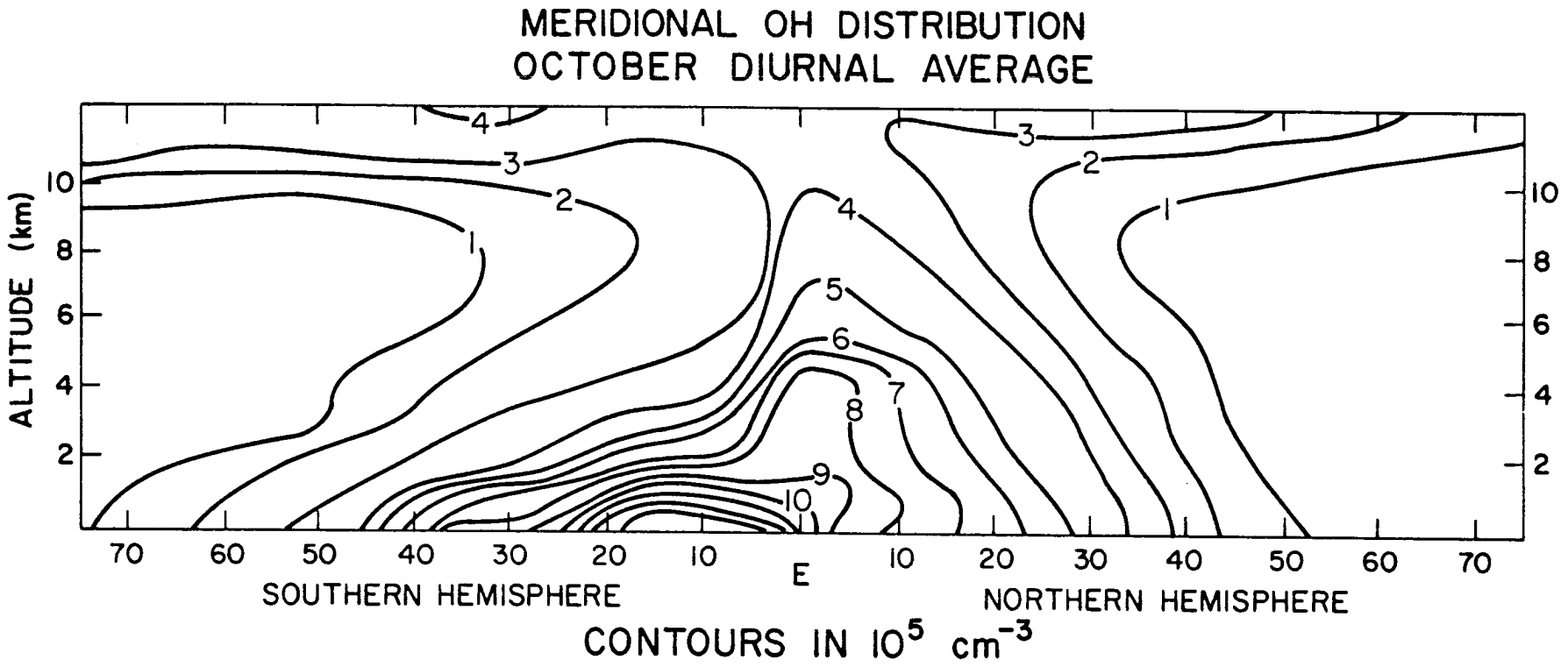
MERIDIONAL OH DISTRIBUTION
OCTOBER DIURNAL AVERAGE
ALTITUDE (km)
10
8
6
4
2
1
2
3
4
5
6
7
8
9
10
70 60 50 40 30 20 10
E
10 20 30 40 50 60 70
SOUTHERN HEMISPHERE
NORTHERN HEMISPHERE
CONTOURS IN 10^5 cm^{-3}

Fig. 10d

what is found in the winter season). The high values found above 9 kms during the summer season at high latitudes can be attibuted to the very high concentrations of stratospheric ozone and the fact that these latitudes are in sunlight throughout most of the day at this time of the year.

Figures 10e, f, g, and h are presented for comparison with the few daytime OH measurements that are available. Davis et al. (1976) have observed OH number densities between 3 and 8 x 10^6 cm^{-3} in October, 1975, during daytime clean air conditions between 21°N and 32°N in the mid- and upper troposphere. The values computed (Fig. 10h) in this study are about five times lower than Davis et al. (1976) have observed. Near the surface, Perner et al. (1976) measured between 0 and 7 x 10^6 cm^{-3} in Julich, Germany (51°N), in late summer and early autumn. Unfortunately, their detection limit was 4 x 10^6 cm^{-3}, and no OH was observed in most cases. Their finding that OH generally remains below this level is not inconsistent with our results. Lastly, the preliminary results of Campbell (1977), taken near the surface at Pullman, Washington (47°N), in August and October, 1977, range between 2 and 8 x 10^5 cm^{-3} which are in relatively good agreement with this study's calculations. Unfortunately, none of the observations have concurrent measurements of ozone, water vapor, carbon monoxide, nitric oxide, nitrogen dioxide and incoming solar radiation--all of which are quite variable and have an important effect on the model-derived OH. Therefore, it is difficult to assess the model's ability to simulate OH number densities accurately based on these few measurements and its is necessary to employ other considerations to determine the validity of the output of the model.

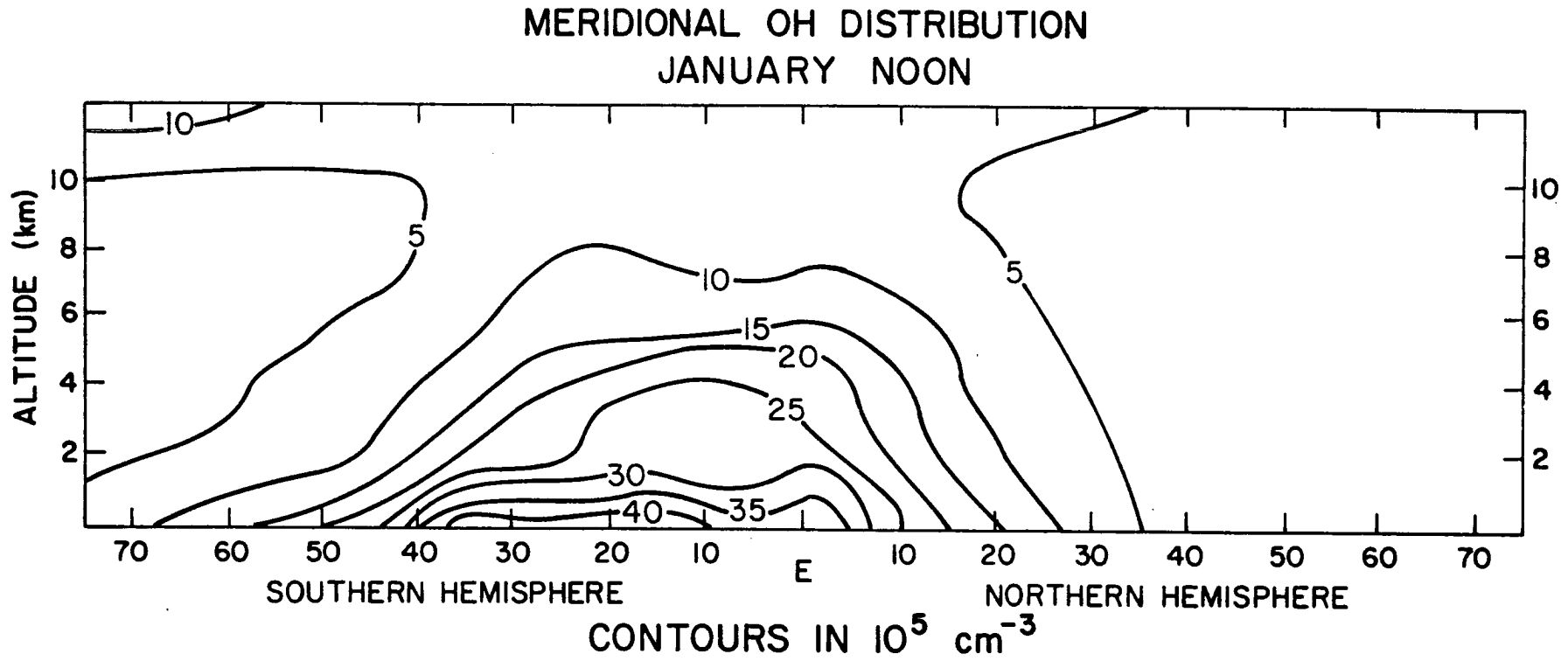
MERIDIONAL OH DISTRIBUTION
JANUARY NOON
ALTITUDE (km)
10
8
6
4
2
10
5
10
15
20
25
30
35
40
5
70 60 50 40 30 20 10 E 10 20 30 40 50 60 70
SOUTHERN HEMISPHERE
NORTHERN HEMISPHERE
CONTOURS IN 10^5 cm^{-3}

Fig. 10e

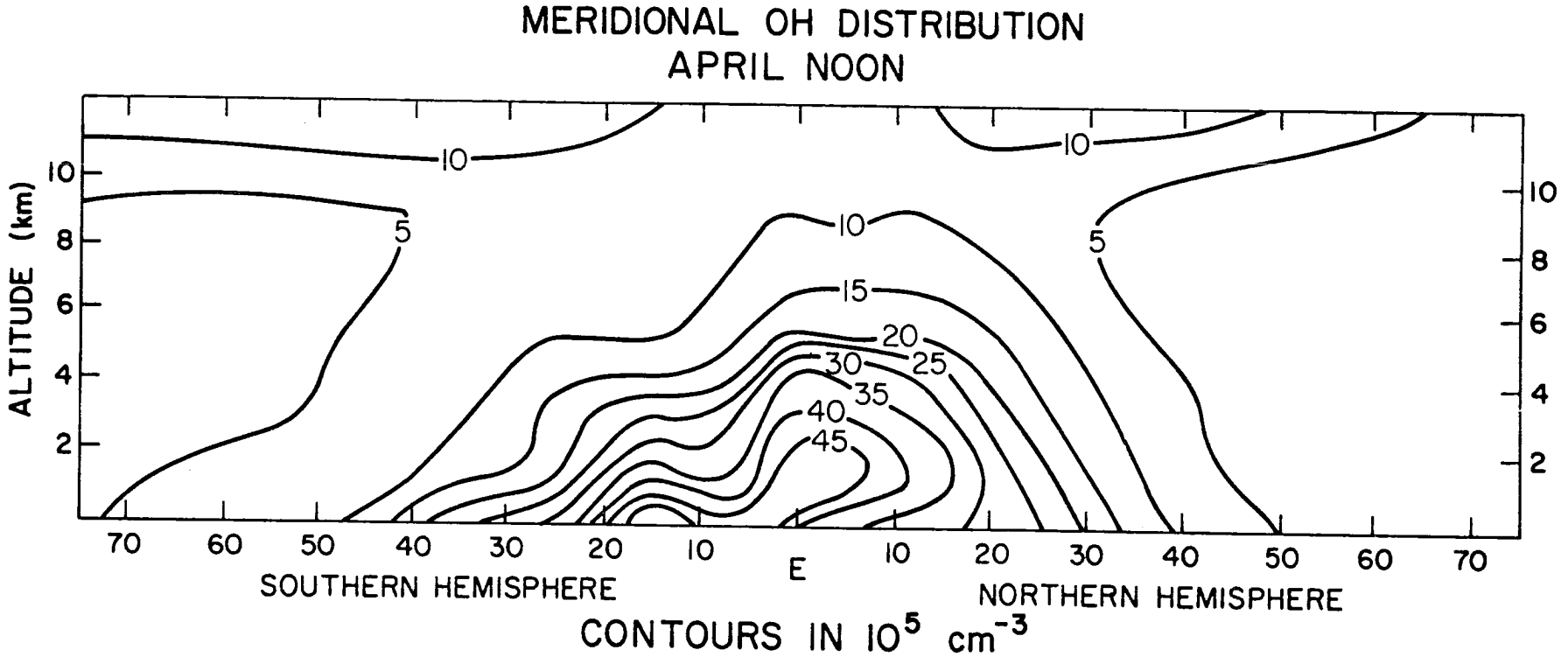
MERIDIONAL OH DISTRIBUTION
APRIL NOON
ALTITUDE (km)
10
8
6
4
2
5
10
15
20
25
30
35
40
45
70 60 50 40 30 20 10 E 10 20 30 40 50 60 70
SOUTHERN HEMISPHERE
NORTHERN HEMISPHERE
CONTOURS IN 10^5 cm^{-3}

Fig. 10f

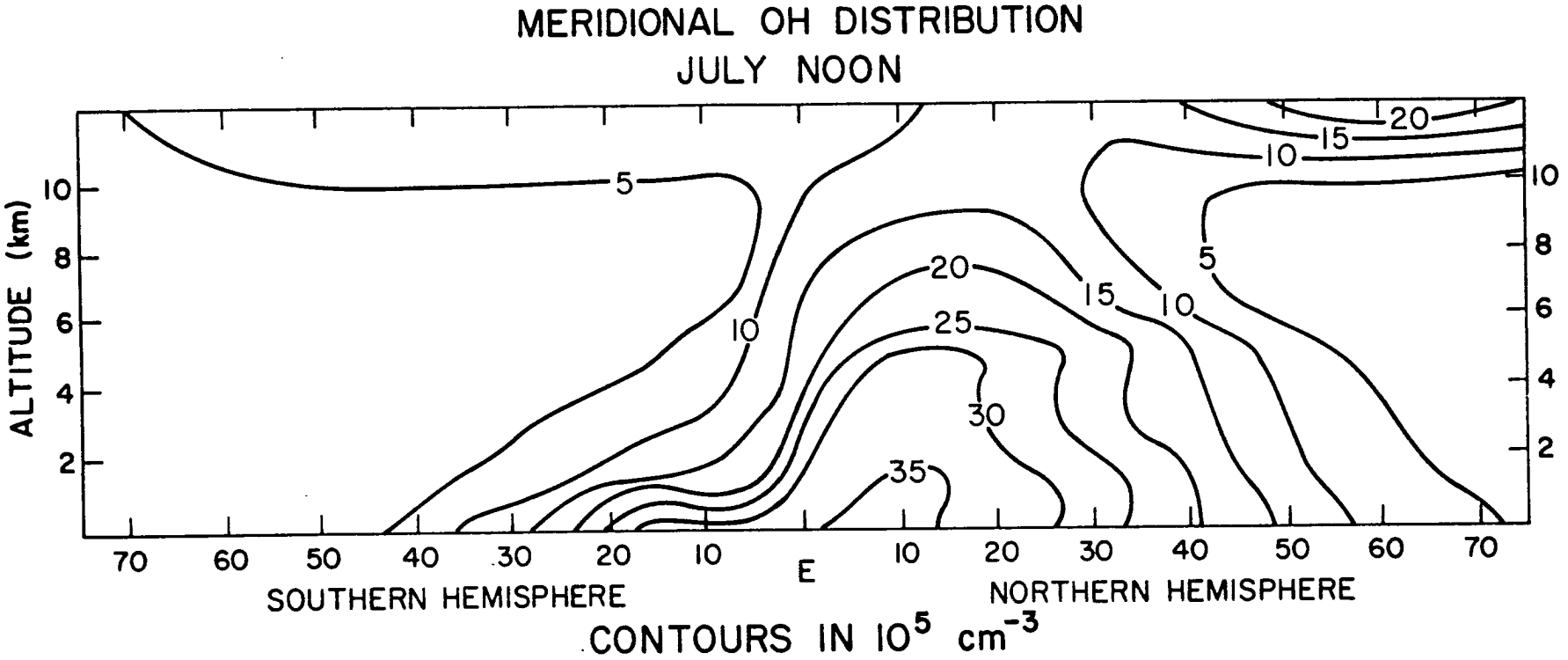
MERIDIONAL OH DISTRIBUTION
JULY NOON
ALTITUDE (km)
10
8
6
4
2
5
10
20
25
30
35
15
20
10
5
70
60
50
40
30
20
10
E
10
20
30
40
50
60
70
SOUTHERN HEMISPHERE
NORTHERN HEMISPHERE
CONTOURS IN 10^5 cm^{-3}

Fig. 10g

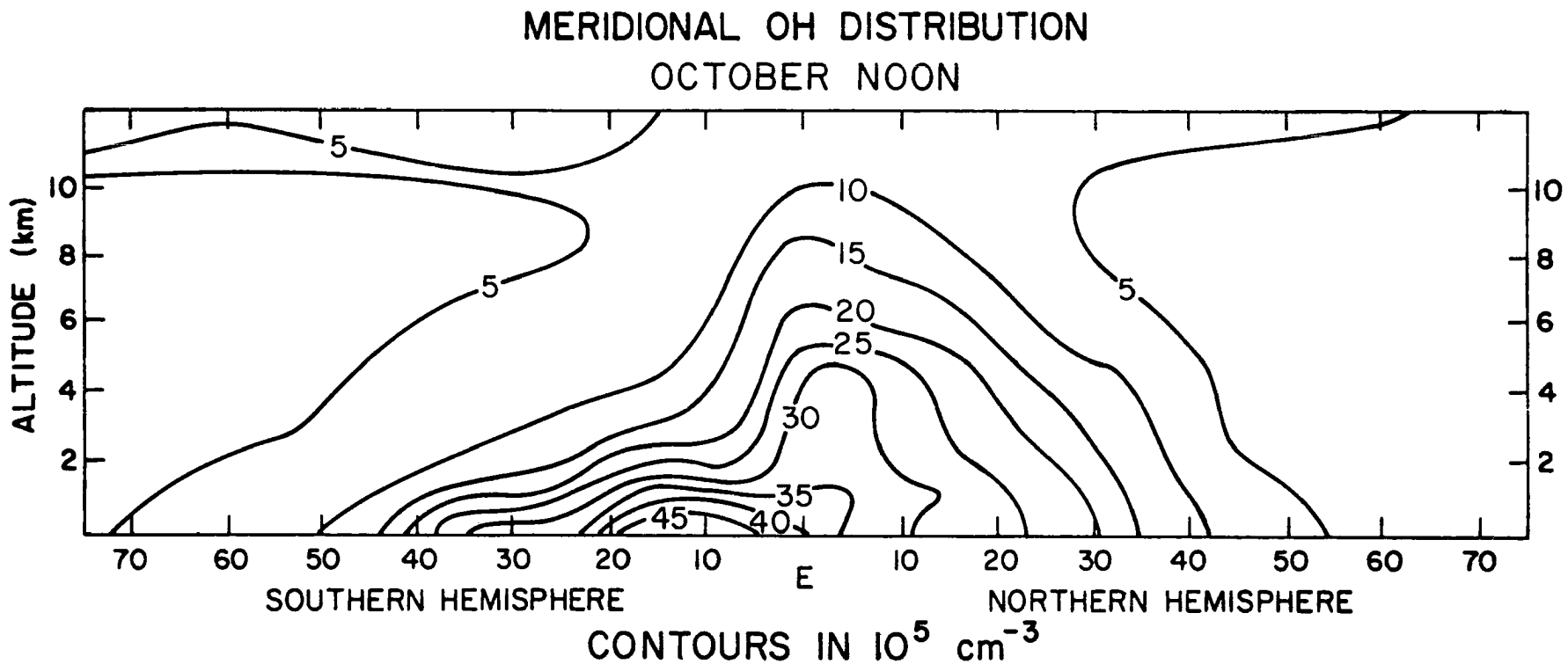
MERIDIONAL OH DISTRIBUTION
OCTOBER NOON
ALTITUDE (km)
10
8
6
4
2
5
5
10
15
20
25
30
35
45
40
5
70 60 50 40 30 20 10 E 10 20 30 40 50 60 70
SOUTHERN HEMISPHERE
NORTHERN HEMISPHERE
CONTOURS IN 10^5 cm^{-3}

Fig. 10h

The most striking difference between the two hemispheres is the difference in the vertical gradients of OH. Figure 11 shows the yearly averaged OH profiles for both hemispheres which clearly depicts this difference. Although the Southern Hemisphere's lower troposphere values are considerably higher, the profiles cross at an altitude near 2 kms at which point more OH is seen in the Northern Hemisphere's mid- and upper troposphere. These higher values can be attributed to the higher tropospheric ozone concentrations found in this region. Again, it is interesting to note the very similar values found in the upper troposphere. Above 9 kms, OH begins to increase due to the enhanced ozone levels at most latitudes. The slight increase in Northern Hemisphere OH compared to Southern Hemisphere upper troposphere OH values is brought about by the slightly warmer temperatures in this region. Because conventional radiosonde dew point data were not available for these altitudes, water vapor concentrations were computed from relative humidity information (U.S. Standard Atmosphere Supplement, 1966) in the upper troposphere. Although the relative humidity was equal in both hemispheres, the warmer temperatures in the Northern Hemisphere resulted in a higher H_2O number density. Thus, OH production via R1 is enhanced, yielding slightly higher OH concentrations.

Although much more can be said about the model-derived OH results presented in Figs. 9, 10, and 11, we conclude that such a discussion would be speculative at this time since the results of our computations are quite sensitive to model assumptions. Therefore, we feel that the focus of this discussion should be to examine some of the key factors which had to be prescribed in the calculations and the sensitivity of the results to these assumptions.

SEASONALLY AND DIURNALLY AVERAGED OH PROFILES FOR THE NORTHERN AND SOUTHERN HEMISPHERE

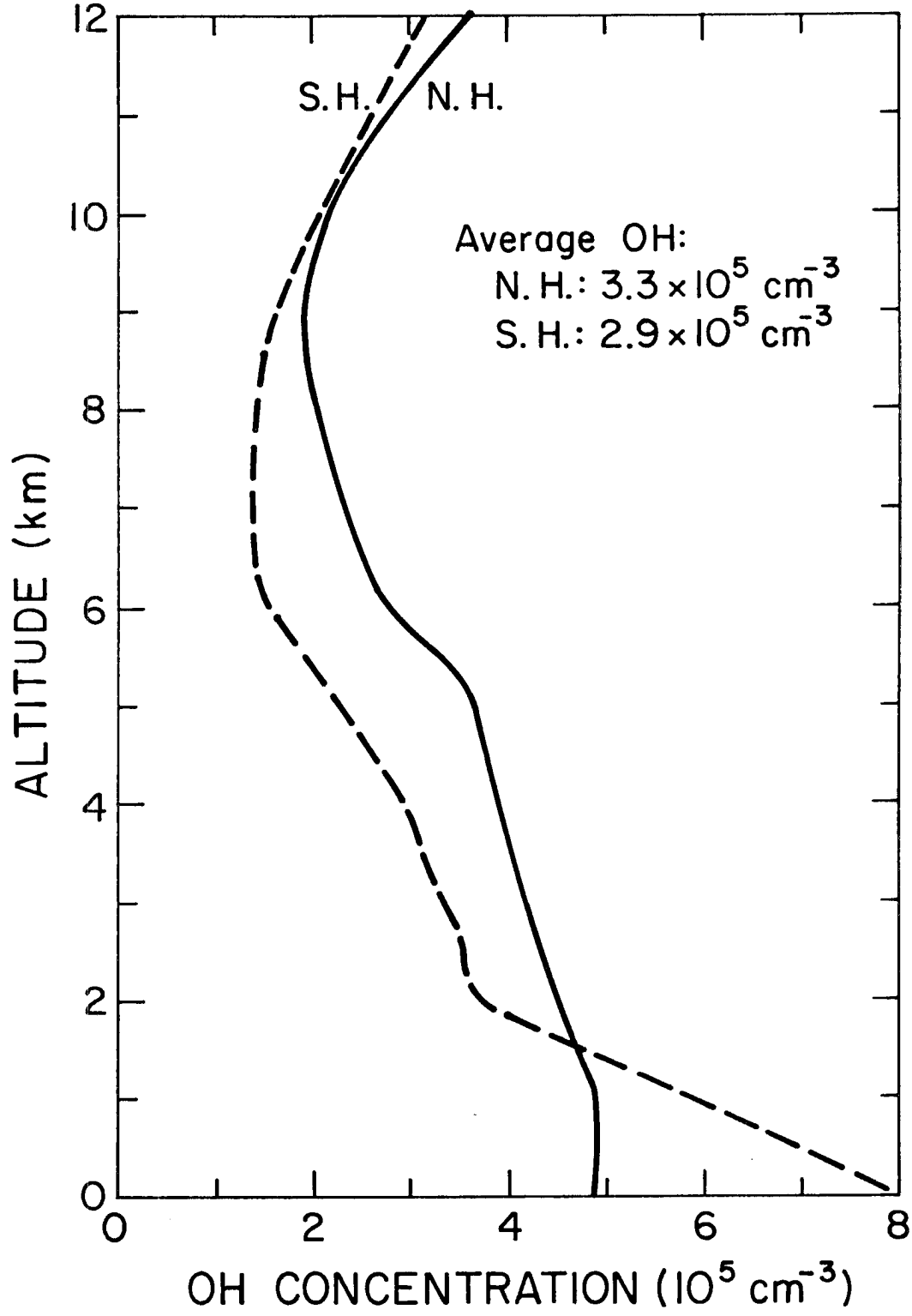

Fig. 11

Because of the relatively few observations of the nitrogen oxides ($NO_x = NO + NO_2$) in the "clean" troposphere, the uncertainty surrounding the prescription of the concentrations of these gases must be examined in detail. Noxon (1977) presents the argument that the column abundance of NO_2 in the troposphere is less than 5×10^{14} cm^{-2} but that a true value of the column density on a global scale still is not known. Three points which hinder the assessment of true global values are:

1. the definition of "unpolluted" air;
2. the influence of polluted air on average tropospheric values; and
3. the observation of NO_2 tropospheric column densities below detectable limits.

It therefore becomes quite difficult to assign tropospheric NO and NO_2 profiles that are representative of global averages and we must investigate the effects of these prescribed concentrations on both the computed OH number densities and the overall photochemistry taking place in the troposphere. Lastly, we point out that since Noxon's (1977) measurements were carried out very close to sunrise and sunset, his NO_2 column densities are probably the same as the NO_x column density since the NO to NO_2 ratio,

$$\frac{NO}{NO_2} = \frac{j_{25}}{[O_3] \cdot k_{24}} ,$$

is much less than unity. The remainder of the discussion focuses on the NO_x distribution in the troposphere, keeping in mind that the above ratio is used in the computations.

Figure 12 shows the tropospheric NO_x profiles prescribed in the model calculations which have been presented to this point. Curve A is the NO_x distribution assumed for "clean" tropospheric air and is prescribed

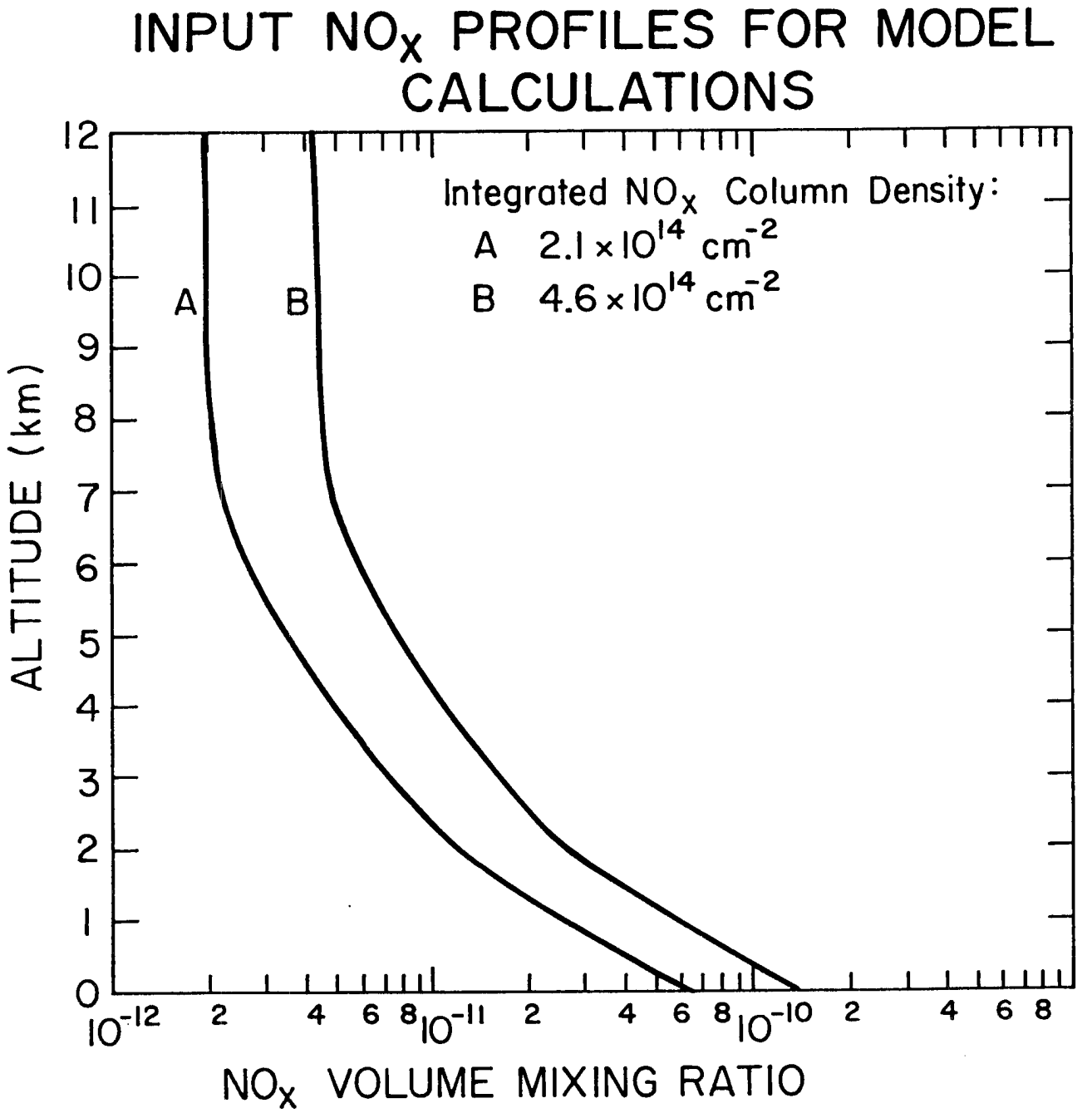
INPUT NOx PROFILES FOR MODEL CALCULATIONS
Integrated NOx Column Density:
A 2.1 x 10^14 cm^-2
B 4.6 x 10^14 cm^-2
A
B
ALTITUDE (km)
0
1
2
3
4
5
6
7
8
9
10
11
12
10^-12
2
4
6
8
10^-11
2
4
6
8
10^-10
2
4
6
8
NOx VOLUME MIXING RATIO

Fig. 12

throughout the Southern Hemisphere and southwards of 15^{o} in the Northern Hemisphere. Curve B is the profile prescribed at 45^{o}N and northward; intermediate profiles are assumed between 15^{o}N and 45^{o}N. The integrated NO_x column density is 2.1×10^{14} cm^{-2} for A and 4.6×10^{14} cm^{-2} for B.

In Fig. 13, we show the sensitivity of calculated OH to assumed tropospheric NO_x distributions. Plotted in this figure are average Northern Hemispheric profiles for July at noon (refer to Fig. 10g) using the following NO_x distributions:

Profile I: NO_x is prescribed according to Fig. 12 (Standard Model);

Profile II: NO_x shown in Fig. 12 is doubled everywhere;

Profile III: NO_x = 0.1 ppb (10^{-10} v v^{-1}) at every point;

Profile IV: NO_x = 0.001 ppb (10^{-12} v v^{-1}) at every point.

Doubling the amount of NO_x increases the average OH in the Northern Hemisphere by 20% from 3.3 to 3.9×10^{5} cm^{-3}. By letting the NO_x mixing ratio equal 0.1 ppb (Profile III), the total amount of tropospheric NO_x is increased by a factor of 6.5 over the amount of tropospheric NO_x used to generate Profile I; although only slightly more NO_x is prescribed at the surface, a fifty-fold increase in NO_x is seen in the low-latitude upper troposphere. The net result of this relatively high prescription of NO_x is that the average Northern Hemisphere OH is increased to 9.5×10^{5} cm^{-3} (192% increase over Profile I). The implications of such an NO_x distribution in the troposphere will be discussed later. Lastly, by assuming a tropospheric NO_x mixing ratio of 0.001 ppb everywhere, the OH distribution depicted by Profile IV is produced. Thus, it is clear from Fig. 13 that a wide variation of tropospheric OH can be calculated

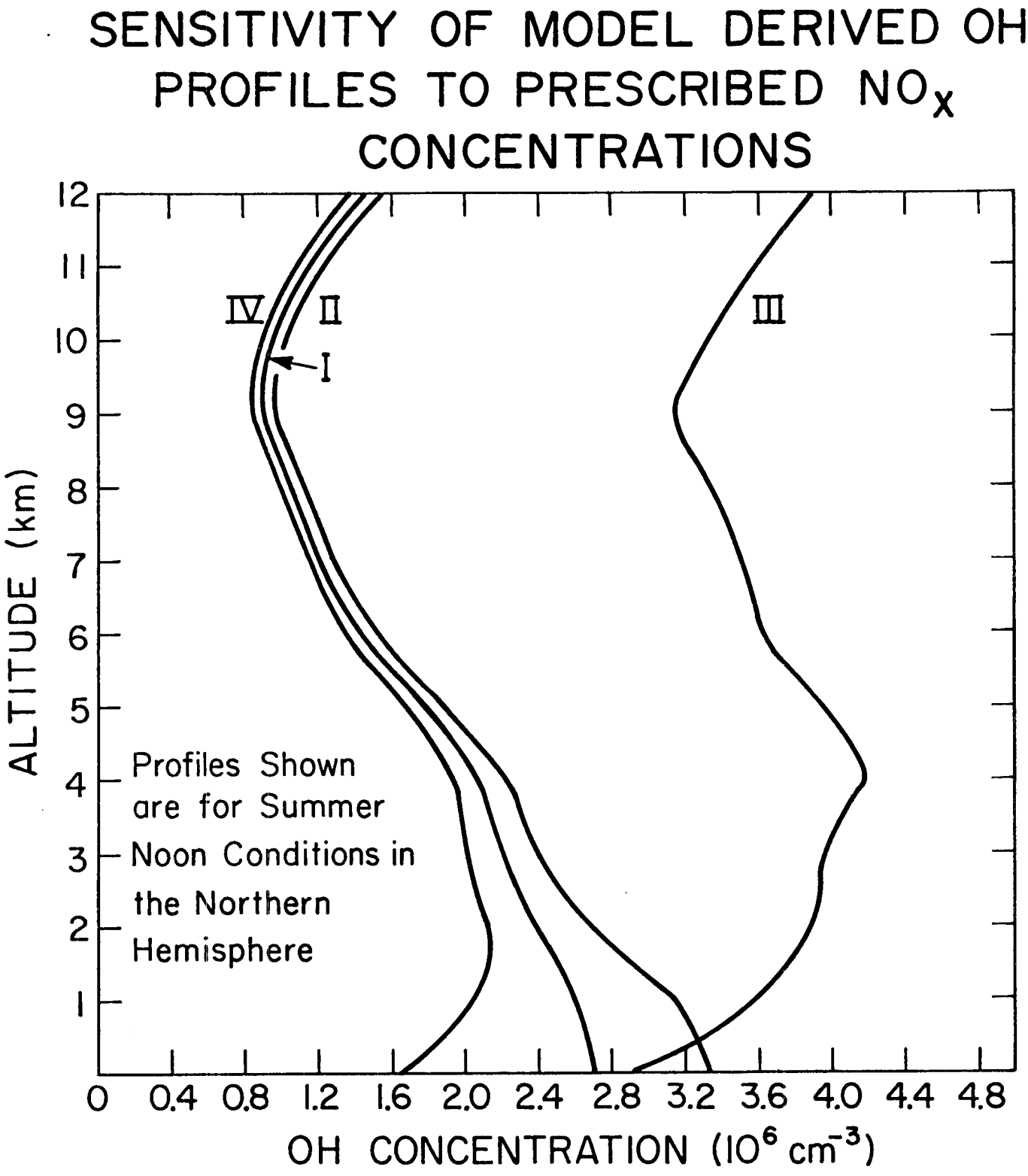
SENSITIVITY OF MODEL DERIVED OH PROFILES TO PRESCRIBED NO_x CONCENTRATIONS
ALTITUDE (km)
12
11
10
9
8
7
6
5
4
3
2
1
IV
II
I
III
Profiles Shown are for Summer Noon Conditions in the Northern Hemisphere
0
0.4
0.8
1.2
1.6
2.0
2.4
2.8
3.2
3.6
4.0
4.4
4.8
OH CONCENTRATION (10^6 cm^{-3})

Fig. 13

from the different prescriptions of NO_x. In addition to the relatively few observations of NO and NO_2, consideration of the tropospheric budgets of other gases (namely, CO and O_3) must be used in the determination of the "correct" tropospheric NO_x distribution. Although little is known about the latitudinal and height distributions of NO and NO_2, the budget analyses do give a crude estimate of how much total NO_x in the troposphere is necessary to be consistent with our present understanding of these budgets.

Table 2 summarizes some of the photochemical calculations in the Northern Hemisphere for the four NO_x distributions described above. In general, the more NO_x present enhances not only the concentration of OH, but the amount of carbon monoxide oxidized [from $CO + OH(+M) \rightarrow CO_2 + H(+M)$] and the amount of methane oxidized ($CH_4 + OH \rightarrow CH_3 + H_2O$). Particularly noteworthy is the fact that both CO and CH_4 oxidation lead to the production of ozone in the troposphere (see Crutzen, 1974; Fishman and Crutzen, 1977), and upper limits on the photochemical production of tropospheric ozone can readily be determined.

Catalytic production of ozone initiated by OH attack on carbon monoxide occurs through the reaction sequence:

R9a(b)	$CO + OH(+M) \rightarrow CO_2 + H(+M)$
R30	$H + O_2 + M \rightarrow HO_2 + M$
R14	$HO_2 + NO \rightarrow OH + NO_2$
R25	$NO_2 + h\nu \rightarrow NO + O$
R28	$O + O_2 + M \rightarrow O_3 + M$
	$CO + 2\ O_2 + h\nu \rightarrow CO_2 + O_3$

Based on what we presently know about tropospheric photochemistry, the only reaction in this chain that may not possibly occur nearly 100%

TABLE 2

Sensitivity of Model Calculations to Prescribed NO_x Concentrations for the Northern Hemisphere

Profile	I Standard	II Double NO_x of I	III NO_x = 0.1 ppb	IV NO_x = 0.001 ppb
Tropospheric NO_x Column Density (10^{14} cm^{-2})	3.4	6.8	22.9	0.2
Average OH (10^5 cm^{-3})	3.3	3.9	9.5	2.9
CO Oxidation (10^{11} mol cm^{-2} s^{-1})	2.4	3.0	8.5	1.8
CH_4 Oxidation (10^{11} mol cm^{-2} s^{-1})	0.4	0.6	1.0	0.4
Upper Limit O_3 Production (10^{11} mol cm^{-2} s^{-1})	3.5	4.4	10.9	2.8
O_3 Efficiency Production Factor	0.50	0.75	0.92	0.03
Tropospheric O_3 Production by Photochemistry (10^{11} mol cm^{-2} s^{-1})	1.8	3.3	10.0	0.1
Tropospheric O_3 Destruction by Photochemistry (10^{11} mol cm^{-2} s^{-1})	1.2	1.2	1.4	1.2
Net Photochemical O_3 Production (10^{11} mol cm^{-2} s^{-1})	+0.6	+2.1	+8.6	-1.1

Estimated O_3 Destruction at the Ground (10^{11} mol cm^{-2} s^{-1}) 0.4-0.8

of the time is R14. In other words, we can assume that every H produced from R9 will become HO_2 and that every NO_2 produced through R14 will photolyze to give atomic oxygen which, in turn, will find an oxygen molecule to make ozone.

An examination of Fig. 1 and Table 1 shows that the following reactions involving HO_2 are most likely to take place in the troposphere:

R14 $NO + HO_2 \rightarrow NO_2 + OH$,

R15 $O_3 + HO_2 \rightarrow 2\ O_2 + OH$,

R17 $OH + HO_2 \rightarrow H_2O + O_2$,

R20 $HO_2 + HO_2 \rightarrow H_2O_2 + O_2$, and

R20a $CH_3O_2 + HO_2 \rightarrow CH_3O_2H + O_2$.

Using representative tropospheric concentrations and atmospheric conditions, we can look at which of the above reactions occurs most frequently; these are summarized in Table 3. The numbers show that even in an atmosphere in which NO_x concentrations are very low (<0.1 ppb), the $NO + HO_2$ reaction determines the fate of the HO_2 radical. However, it is clear that the percentage of HO_2 that follows the R14 path depends on the assumed NO concentration, the computed radical concentrations (OH, HO_2 and CH_3O_2) and the background ozone concentration. On the other hand, because of the extremely fast value of k_{14} (Howard and Evenson, 1977), it is also quite evident that the other HO_2 reactions do not determine the path of HO_2 until NO_x mixing ratios go below 0.01 ppb. Note that our model-assumed NO_x profile (Fig. 12) does prescribe NO_x mixing ratios less than this value above an altitude of 4 kms.

A similar examination of ozone production from methane oxidation can be made, but the conclusion is the same: the amount of ozone produced

TABLE 3

Competition of Reactions Involving the HO_2 Radical for Representative Tropospheric Conditions

Reaction	Reactant Concentration	Rate Constant	Rate of Reaction	Fraction
$HO_2 + NO \rightarrow OH + NO_2$	1×10^{9} cm^{-3} ($\sim$0.04 ppb)	8×10^{-12}	8×10^{-3}	0.89
$HO_2 + O_3 \rightarrow OH + 2\ O_2$	1×10^{12} cm^{-3} ($\sim$40 ppb)	4×10^{-16}	4×10^{-4}	0.05
$HO_2 + OH \rightarrow H_2O + O_2$	4×10^{6} cm^{-3}	5×10^{-11}	2×10^{-4}	0.02
$HO_2 + HO_2 \rightarrow H_2O_2 + O_2$	4×10^{8} cm^{-3}	8x10-13	3×10^{-4}	0.03
$CH_3O_2 + HO_2 \rightarrow CH_3O_2H + O_2$	2×10^{8} cm^{-3}	8×10^{-13}	1×10^{-4}	0.01

from methane oxidation is dependent on the background concentration of the nitrogen oxides. Although the methane oxidation chemistry is more complex than CO oxidation (see Crutzen, 1974), we will assume in this study that no more than 2.5 ozone molecules can be produced from each CH_4 + OH reaction. The ratio of O_3 produced to CH_4 oxidized is most dependent of the photolytic path of formaldehyde (CH_2O). If CH_2O photodissociates completely to H + CHO (R7a), as many as four ozone molecules from each methane molecule oxidized could be produced. However, using the dissociation rates shown in Table 1 for j_{7a} and j_{7b}, only 2.5 ozone molecules are produced from the OH attack on CH_4. For the four cases given in Table 2, CO oxidation dominates CH_4 oxidation by at least a factor of 5; therefore, the contribution to the upper limit of the amount of ozone produced by CO oxidation is at least twice as great as the ozone produced from CH_4 oxidation. Thus, the quantity presented in Table 2 under the category of "O_3 Production (Upper limit)" is the sum of "CO Oxidation" and 2.5 times "CH_4 Oxidation."

From the actual model results, one can determine the true "ozone efficiency production factor" for each of the four NO_x input distributions. For the examples presented here, this factor ranges from 0.03 where the NO_x mixing ratio is 0.001 ppb, to 0.92 where a 0.1 ppb NO_x mixing ratio is prescribed everywhere. Thus, it is important to note that both the upper limit of the amount of ozone production and the efficiency of the ozone production is increased when more NO_x is present. An important consequence of these calculations is that the amount of tropospheric ozone which is likely to be produced from photochemistry ($\sim 1 \times 10^{12}$ mol cm^{-2} s^{-1}) when the NO_x mixing ratio of 0.1 ppb (or greater) everywhere in the troposphere is greatly out of line with previous

TABLE 3

Competition of Reactions Involving the HO_2 Radical for Representative Tropospheric Conditions

Reaction	Reactant Concentration	Rate Constant	Rate of Reaction	Fraction
$HO_2 + NO \rightarrow OH + NO_2$	1×10^{9} cm^{-3} ($\sim$0.04 ppb)	8×10^{-12}	8×10^{-3}	0.63
$HO_2 + O_3 \rightarrow OH + 2\ O_2$	1×10^{12} cm^{-3} ($\sim$40 ppb)	4×10^{-16}	4×10^{-4}	0.03
$HO_2 + OH \rightarrow H_2O + O_2$	4×10^{6} cm^{-3}	5×10^{-11}	2×10^{-4}	0.02
$HO_2 + HO_2 \rightarrow H_2O_2 + O_2$	3×10^{8} cm^{-3}	8×10^{-12}	2×10^{-3}	0.19
$CH_3O_2 + HO_2 \rightarrow CH_3O_2H + O_2$	2×10^{8} cm^{-3}	8×10^{-12}	2×10^{-3}	0.13

from methane oxidation is dependent on the background concentration of the nitrogen oxides. Although the methane oxidation chemistry is more complex than CO oxidation (see Crutzen, 1974), we will assume in this study that no more than 2.5 ozone molecules can be produced from each CH_4 + OH reaction. The ratio of O_3 produced to CH_4 oxidized is most dependent of the photolytic path of formaldehyde (CH_2O). If CH_2O photodissociates completely to H + CHO (R7a), as many as four ozone molecules from each methane molecule oxidized could be produced. However, using the dissociation rates shown in Table 1 for j_{7a} and j_{7b}, only 2.5 ozone molecules are produced from the OH attack on CH_4. For the four cases given in Table 2, CO oxidation dominates CH_4 oxidation by at least a factor of 5; therefore, the contribution to the upper limit of the amount of ozone produced by CO oxidation is at least twice as great as the ozone produced from CH_4 oxidation. Thus, the quantity presented in Table 2 under the category of "O_3 Production (Upper limit)" is the sum of "CO Oxidation" and 2.5 times "CH_4 Oxidation."

From the actual model results, one can determine the true "ozone efficiency production factor" for each of the four NO_x input distributions. For the examples presented here, this factor ranges from 0.03 where the NO_x mixing ratio is 0.001 ppb, to 0.92 where a 0.1 ppb NO_x mixing ratio is prescribed everywhere. Thus, it is important to note that both the upper limit of the amount of ozone production and the efficiency of the ozone production is increased when more NO_x is present. An important consequence of these calculations is that the amount of tropospheric ozone which is likely to be produced from photochemistry ($\sim 1 \times 10^{12}$ mol cm^{-2} s^{-1}) when the NO_x mixing ratio of 0.1 ppb (or greater) everywhere in the troposphere is greatly out of line with previous

estimates of the tropospheric ozone budget (Fishman and Crutzen, 1977; Chameides and Stedman, 1977; Fabian and Pruchniewicz, 1977). Furthermore, the amount of ozone destroyed photochemically does not vary appreciably from 1×10^{11} mol. cm^{-2} s^{-1} since this quantity is primarily fixed by the amount of ozone lost through R1 and does not depend on any concentrations other than those of ozone and water vapor. Thus, an efficient ozone destruction mechanism presently not considered in any tropospheric ozone budget must dominate the ozone sink if so much tropospheric ozone is produced when an 0.1 ppb NO_x mixing ratio is present everywhere in the troposphere. Presently we cannot speculate on such a destruction process and therefore conclude that such a high NO_x mixing ratio probably does not exist in the troposphere.

On the other hand, the NO_x distribution depicted in Fig. 12 does yield a tropospheric ozone budget which can be said to be in reasonable agreement with what is believed to the tropospheric ozone budget. In addition, these NO_x concentrations are consistent with the tropospheric NO_x column density observations of Noxon (1977) and the surface NO observations of Drummond (1977) for "clean" air in Wyoming.

Similarly, a tropospheric ozone budget for the Southern Hemisphere can be derived. In these calculations, the NO_x concentrations depicted by Curve A in Fig. 12 is prescribed at all latitudes (see Table 4). Comparing the photochemistry occurring in both hemispheres using this particular set of model-derived results, two very general conclusions are made:

1. the net photochemical production of ozone in the Northern Hemisphere troposphere may be comparable or even greater than the amount of ozone coming through the tropopause (Danielsen and Mohnen, 1977; Fabian and Pruchnienicz, 1977); and

TABLE 4

Model-Derived Tropospheric Budgets

	Northern Hemisphere	Southern Hemisphere
Tropospheric NO_x Column Density ($10^{14}cm^{-2}$)	3.4	2.1
Average OH (10^5 cm^{-3})	3.3	2.9
CO Oxidation	2.4	1.3
CH_4 Oxidation	0.4	0.4
Ozone Production (Upper Limit)	3.5	2.4
Ozone Production Efficiency Factor (Nondimensional)	0.50	0.31
Tropospheric Ozone Produced by Photochemistry	1.8	0.7
Tropospheric Ozone Destroyed by Photochemistry	1.2	0.6
Net Photochemical Ozone Production	+0.6	+0.1
Ozone Destruction at the Ground (from Fabian and Pruchniewicz, 1977)	0.7	0.4

Note: All units are 10^{11} mol cm^{-2} s^{-1}, unless otherwise noted.

2. there seems to be less net photochemical production of ozone taking place in the Southern Hemisphere.

Thus, even if the transport of ozone in both hemispheres were comparable, one would expect to find more ozone in the Northern Hemisphere due to the enhanced photochemical production. Furthermore, the difference in the photochemical production is primarily due to CO oxidation rather than CH_4 oxidation.

Lastly, in this section, we present the global CO budget originally given by Seiler (1974) but updated by the photochemical calculations of our present model (refer to Table 5). Recalling Seiler's CO budget, we note that there was a large degree of uncertainty in the amounts of CO produced and destroyed photochemically: 15-40 x 10^{14} g yr^{-1} produced from methane oxidation and 19-50 x 10^{14} g yr^{-1} destroyed by OH-attack. Furthermore, we observe that these mechanisms greatly dominate all other source and sink terms in Seiler's budget.

Using our model-derived results, on the other hand, the amount of CO produced from methane oxidation is only about half as large as the contribution from Seiler's anthropogic estimate. In addition, we note that the number we give under the "CH_4 + OH" leading in Table 3 (3.3 x 10^{14} g yr^{-1}) is an upper limit to the amount of CO produced photochemically since we must assume that every CH_4 oxidized results in a CO molecule produced. This assumption may not be valid if some of the peroxides or the formaldehyde produced as intermediate products of methane oxidation are rapidly removed by heterogeneous processes. Since the methane concentration is well known everywhere in the troposphere (Ehhalt, 1974), photochemical production of carbon monoxide can be increased only if the tropospheric concentrations of OH are increased.

TABLE 5

Global Carbon Monoxide Budget

(from Seiler, 1974, and modified by this study)

Sources (10^{14} g yr^{-1})	Global	Northern Hemisphere	Southern Hemisphere
Anthropogenic	6.4	5.4	1.0
Oceans	1.0	0.4	0.6
Forest Burning	0.6	0.4	0.2
Oxidation of Hydrocarbons	0.6	0.4	0.2
CH_4 + OH (this study)	3.3	1.7	1.6
Total	11.9	8.3	3.6
Sinks (10^{14} g yr^{-1})			
Soil Uptake	4.5	3.0	1.5
Into Stratosphere	1.1	0.9	0.2
CO + OH (this study)	13.9	8.9	5.0
Total	19.5	12.8	7.7
Net	-7.6 (Budget does not balance)		

However, for every OH present, more than five times CO is destroyed by OH-attack than is produced via methane oxidation. Thus, the imbalance shown in Table 5 would become worse if the average amount of OH were increased and that a revision of Seiler's budget must be considered. In future research efforts, we will examine the possibility that CO can be released by soils under certain conditions and that the amount of carbon monoxide produced by the oxidation of natural and anthropogenic hydrocarbons may be higher than Seiler had estimated.

Another fundamental unknown in atmospheric chemistry is the rate of removal of atmospheric gases by processes other than gas-phase reactions. In the present study, three gases are included in the model whose concentrations are not prescribed and which may be removed more efficiently by heterogeneous reactions than by homogeneous ones. Of these species (HNO_3, H_2O_2, and CH_3O_2H), the tropospheric fate of hydrogen peroxide, H_2O_2, is the most critical in the calculation of the OH number density.

The method adopted for heterogeneous removal of these gases is similar to the one prescribed by Fishman and Crutzen (1977). A removal rate (s^{-1}) is defined for the lowest five kms of the troposphere and then falls off exponentially above that level to 12 kms according to the formula:

$$k(z)_{HET} = k^{o}_{HET} \exp^{[-0.46(z-5)]}, \quad z > 5 \text{ km},$$

$$k(z)_{HET} = k^{o}_{HET}, \quad z \leq 5 \text{ km},$$

where k(z) is the heterogeneous removal rate at altitude z, and k^{o}_{HET} is the prescribed heterogeneous removal rate below 5 kms. The exponential decay with height reproduces the observations of Davidson et al. (1966) for removal of radioactive debris.

The prescription of k^{o}_{HET} does influence the model calculations and the sensitivity of the computations to this parameter is presented in Figures 14, 15, and Table 6. As expected, a faster heterogeneous removal rate depletes the abundance of both H_2O_2 and OH since hydrogen peroxide acts as a reservoir for odd hydrogen species in the lower atmosphere. The primary problem to be resolved is to choose the correct value of k^{o}_{HET} for the model calculations. The three values discussed here are 2×10^{-5} s^{-1} which was used for the "standard" model calculations (Profile A in Figures 14 and 15), 5×10^{-6} s^{-1} (Profile B), and 2.4×10^{-6} s^{-1} (Profile C). Unfortunately, observations of hydrogen peroxide in the unpolluted atmosphere do not exist and it is therefore impossible to tune this removal rate (which is the primary loss mechanism for H_2O_2) to measurements. Thus, other considerations must be taken into account for the proper prescription of k^{o}_{HET}.

The most widely investigated gas whose fate is primarily controlled by heterogeneous processes is sulfur dioxide. In prior studies, the residence times computed for SO_2 vary by more than an order of magnitude from five days (Junge, 1960) to less than half a day (Eliassen and Saltbones, 1975; Metham, 1950). These values yield removal rates of 2.3×10^{-6} s^{-1} and 2.3×10^{-5} s^{-1}, respectively. Whereas the above studies used emission data and measurements to derive residence time, Henmi et al. (1977) compute SO_2 residence times over the eastern United States using climatological data of the mixing layer height, precipitation information and the consideration of microphysical cloud processes to produce a "scavenging" coefficient between 1 and 4×10^{-5} s^{-1} (SO_2 residence times between 6 and 24 hours). Thus, since any of the three removal rates summarized in Table 6 could be used justifiably in the calculations, other considerations must be examined.

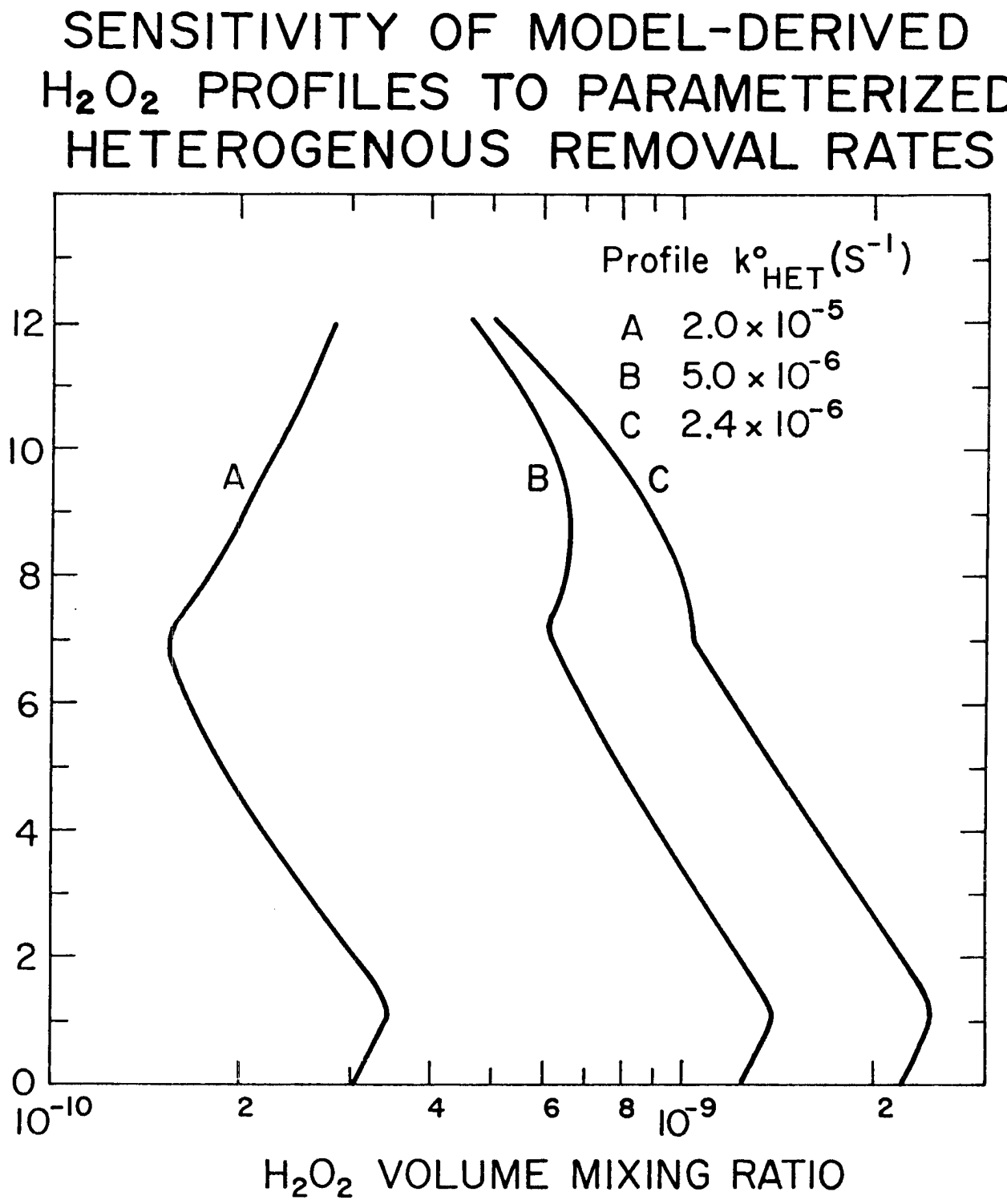
SENSITIVITY OF MODEL-DERIVED
H2O2 PROFILES TO PARAMETERIZED
HETEROGENOUS REMOVAL RATES
Profile k°HET(S-1)
A 2.0 x 10-5
B 5.0 x 10-6
C 2.4 x 10-6
A
B
C
12
10
8
6
4
2
0
10-10
2
4
6
8
10-9
2
H2O2 VOLUME MIXING RATIO

Fig. 14

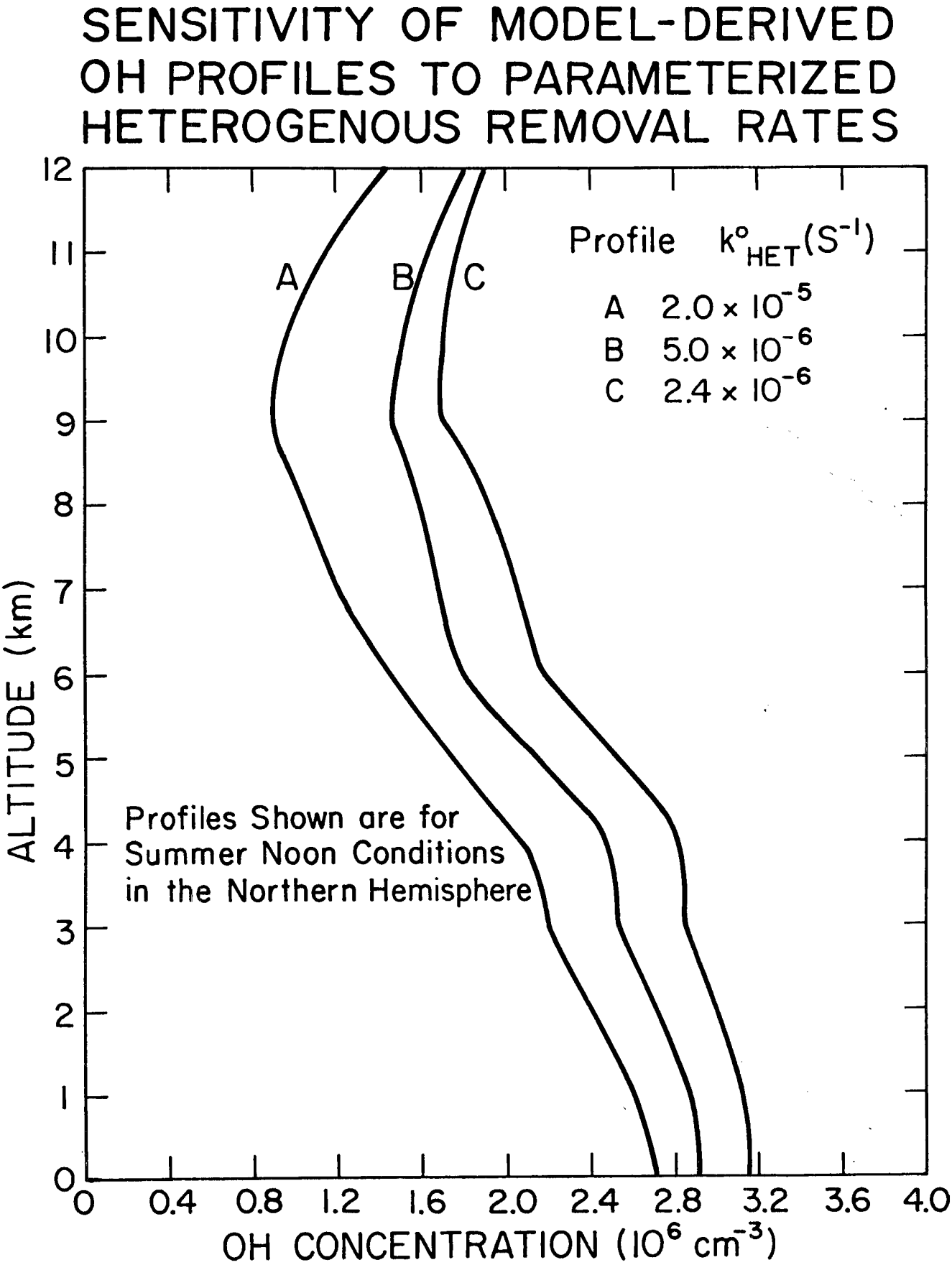
SENSITIVITY OF MODEL-DERIVED OH PROFILES TO PARAMETERIZED HETEROGENOUS REMOVAL RATES
Profile $k^{o}_{HET}(S^{-1})$
A 2.0×10^{-5}
B 5.0×10^{-6}
C 2.4×10^{-6}
A
B
C
Profiles Shown are for Summer Noon Conditions in the Northern Hemisphere
ALTITUDE (km)
OH CONCENTRATION (10^{6} cm^{-3})
0
1
2
3
4
5
6
7
8
9
10
11
12
0
0.4
0.8
1.2
1.6
2.0
2.4
2.8
3.2
3.6
4.0

Fig. 15

VI. TROPOSPHERIC RESIDENCE TIME OF METHYL CHLOROFORM

Because of increased usage of methyl chloroform (CH_3CCl_3) as an industrial solvent, this chemical may become a significant source of chlorine in the stratosphere. According to Crutzen et al. (1977), if the production of CH_3CCl_3 continues to increase at its current rate (∿15% per year), depletion of ozone in the stratosphere due to the chlorine contained in methyl chloroform will exceed the perturbations to the ozone layer by fluorochloromethanes by the end of this century (assuming that the latter's production rates remained fixed at 1975 levels). These estimates, however, are quite sensitive to how much methyl chloroform is removed in the troposphere through OH-attack and thus, it is quite important to know the CH_3CCl_3 removal rate in the troposphere.

Calculations of the methyl chloroform tropospheric residence time before 1977 ranged between 1 and 3 years, and thus it was thought that OH-attack in the troposphere was an efficient enough mechanism to prevent much of it from reaching the stratosphere. However, some recent studies of the global CH_3CCl_3 distribution and its budget (e.g. Singh, 1977b; Chang and Penner, 1977) indicate that a tropospheric residence time on the order of 10 years is more reasonable. This value is consistent with the 10 year residence time computed in this study employing the global OH distribution described earlier.

A summary of the calculations of methyl chloroform residence times is presented in Table 7. With the exception of the study by Cox et al. (1976b), the rate constant for $CH_3CCl_3 + OH \rightarrow CH_2CCl_3 + H_2O$ is very close to 1×10^{-14} cm^3 $mol.^{-1}$ s^{-1} (at 265°K) for the calculations.

TABLE 7

Methyl Chloroform Residence Time Calculations

Study	$k_{CH_3CCl_3 + OH}$	$\overline{OH}$ (Method of Calculation)	Residence Time
Yung et al. (1975)	8.9×10^{-15} ($265^{o}K$)	12×10^{5} (computed)	3 yrs
Cox et al. (1976b)	2.8×10^{-14}	10×10^{5} (assumed)	1 yr
Chang and Wuebbles (1976)	1.4×10^{-14} ($288^{o}K$)	17×10^{5} (computed)	1 yr
Neely and Plonka (1976)	1.0×10^{-14} ($265^{o}K$)	9×10^{5} (inferred)	3 yrs
Singh (1977b)	9.6×10^{-15} ($265^{o}K$)	4×10^{5} (inferred)	8 yrs
Chang and Penner (1977)	$[1.1 \times 10^{-14}]$	3×10^{5} (inferred)	11 yrs
This study	9.6×10^{-15} ($265^{o}K$)	3×10^{5} (computed)	10 yrs

Note: k is in units of cm^3 $mol.^{-1}$ s^{-1}; $\overline{OH}$ is in cm^{-3}.

TABLE 6

Effect of Heterogeneous Removal on Model Calculations

	A	B	C
k^{o}_{HET} (s^{-1})	2.0×10^{-5}	5.0×10^{-6}	2.4×10^{-6}
OH (hemispheric annual average)	3.3×10^{5}	4.8×10^{5}	5.7×10^{5}
H_2O_2 (1 km)	0.34 ppb	1.40 ppb	2.46 ppb
H_2O_2 (10 km)	0.23 ppb	0.62 ppb	0.78 ppb

Justification for employing the relatively fast removal rate used to compute Profile A once again comes from the consideration of global tropospheric budgets. In addition to creating a greater imbalance in the tropospheric carbon monoxide budget by allowing more OH to be present, slower heterogeneous removal rates are inconsistent with the model-prescribed NO_x distribution. Recalling that the average NO_x column abundance in the Northern Hemisphere is 3.4×10^{14} mol. cm^{-2} (see Table 2, Column I) for these calculations, a tropospheric residence time for NO_x can be found if the source strength were known. Anthropogenic input and lightning are believed to be the major sources of NO_x in the troposphere (Chameides et al., 1977; Söderlund and Svenssen, 1976), each contributing a flux in the Northern Hemisphere of about 1×10^{10} mol. cm^{-2} s^{-1}. If we assume an average NO_x flux in the Northern Hemisphere of 2×10^{10} mol. cm^{-2} s^{-1}, the resultant NO_x residence time is $\sim 2 \times 10^4$ s ($\sim$5 hours) producing a removal rate for NO_x of 5×10^{-5} s^{-1}. The current model's OH distribution can remove NO_x at a rate no faster than 2×10^9 mol. cm^{-2} s^{-1}, which means that another NO_x removal process must be taking place at a rate four times faster than gas-phase chemistry. Even the sharp vertical gradient depicted for NO_x in Fig. 12 and the large globally averaged (and probably unrealistic) NO_x deposition velocity of 2 cm s^{-1} still demands that another heterogeneous process is removing NO_x at a rate greater than 10^{10} mol. cm^{-2} s^{-1}. Therefore, in light of the above discussion, it does not seem unreasonable that SO_2, NO_2 and all other tropospheric gases that are susceptible to scavenging processes in the atmosphere (such as HNO_3, H_2O_2, and CH_3O_2H) should be removed rapidly and that $k^o_{HET} = 2 \times 10^{-5}$ s^{-1} is a realistic value. Obviously, more global scale measurements of NO, NO_2, H_2O_2, and HNO_3 are needed to verify this contention.

For some reason, Chang and Wuebbles (1976) used the rate constant expression at 288°K to calculate tropospheric residence times. Evaluating their rate Arrhenius expression at 265°K yields a constant of 8.3×10^{-15} cm^3 $mol.^{-1}$ s^{-1} and a residence time of 2 years. It is interesting to note that the OH calculated directly by previous photo-kinetic models (e.g., Yung et al., 1975 and Chang and Weubbles, 1976) compute OH values that are considerably higher than those computed in this study. The fact that we have used the faster rate constant for the CO + OH reaction given by Chan et al. (1977) may be responsible for lowering the amount of tropospheric OH by nearly a factor of two.

On the other hand, the OH abundance in the troposphere inferred from the various analyses of the methyl chloroform budget (with the exception of the study by Neely and Plonka, 1976) support the lower OH values computed in this study. Furthermore, if there existed an additional methyl chloroform sink in the troposphere other than OH-attack, then the inferred OH abundance would be even lower than the values presented in Table 7. Thus, we point out that the distribution of methyl chloroform and the analysis of its tropospheric budget are consistent with the OH distributions presented in this study and that the lower OH values computed directly are necessary to explain the global carbon monoxide and tropospheric ozone budgets in addition to being in better agreement with what is currently known about methyl chloroform. In summary, we conclude in this section that there is not enough OH in the troposphere to remove methyl chloroform efficiently and that it is likely that a substantial fraction of this chemical released to the atmosphere may find its way into the stratosphere.

VII. THE PRODUCTION RATE OF METASTABLE ATOMIC OXYGEN

Due to the fact that there are only a limited number of tropospheric measurements of OH, much of the discussion in Sections V and VI dealt with trying to reconcile the calculated OH distribution with the tropospheric budgets of ozone, carbon monoxide and methyl chloroform in order to determine the feasibility of such a distribution. Since global averages were used to compute OH in the model, it is felt that such an analysis is more practical than trying to compare local measurements with the calculations because of the likely variability of such observations.

Since the production of hydroxyl radicals in the troposphere primarily takes place through the reaction sequence:

$$\text{R22} \quad O_3 + h\nu \rightarrow O_2 + O(^1D), \text{ and}$$

$$\text{R1} \quad H_2O + O(^1D) \rightarrow 2\ OH,$$

comparison of the model-derived production rate with the measured production rate would provide a useful measure of the model's ability to simulate initial production of odd hydrogen radicals. Assuming that the amount of water vapor and ozone are known through observations, favorable comparison of the computed photolysis rate j_{22} with the measured value of j_{22} would indicate that the initial rate of formation of odd hydrogen radicals is being modelled correctly.

At the National Center for Atmospheric Research in Boulder, Colorado, Russ Dickerson, a graduate student under the direction of Donald Stedman of the Department of Chemistry at the University of Michigan,

is currently measuring j_{22} directly. By placing a transparent bulb filled with nitrous oxide (N_2O) and ozone in sunlight, the following reaction sequence takes place:

$$O_3 + h\nu \rightarrow O(^1D) + O_2, \text{ and}$$
$$O(^1D) + N_2O \rightarrow 2\ NO$$
$$\text{or,} \qquad \rightarrow N_2 + O_2.$$

By knowing the branching ratio of the latter two reactions, one can determine j_{22} by monitoring the amount of NO being produced. Note that there are other reactions taking place in the glass bulb, but that these are properly taken into account. A detailed description of the system is available from Dickerson.

The value of j_{22} computed in the model is calculated through the following expression:

$$j = \int_{290\ nm}^{320\ nm} Q(\lambda)\sigma(\lambda)\Phi(\lambda)d\lambda,$$

where $Q(\lambda)$ is the solar flux (photons $cm^{-2}\ s^{-1}\ nm^{-1}$),

$\sigma(\lambda)$ is the ozone cross section (cm^2),

and $\Phi(\lambda)$ is the quantum yield of $O(^1D)$ from O_3 photolysis.

The effective solar flux at each level of the atmosphere in this wavelength interval is determined from the amount of radiation incident upon the top of the atmosphere, and subsequently from how much of that radiation is absorbed, scatterd, and reflected. The Rayleigh scattering and absorbing properties of the atmosphere are parameterized by an efficient scheme developed by Isaksen et al. (1976).

The input data used for these calculations are presented in Figures 16, 17 and 18. The incoming extraterrestrial radiation between 300 and 320 nm is shown in Figure 16 and is taken from Arvesen et al.

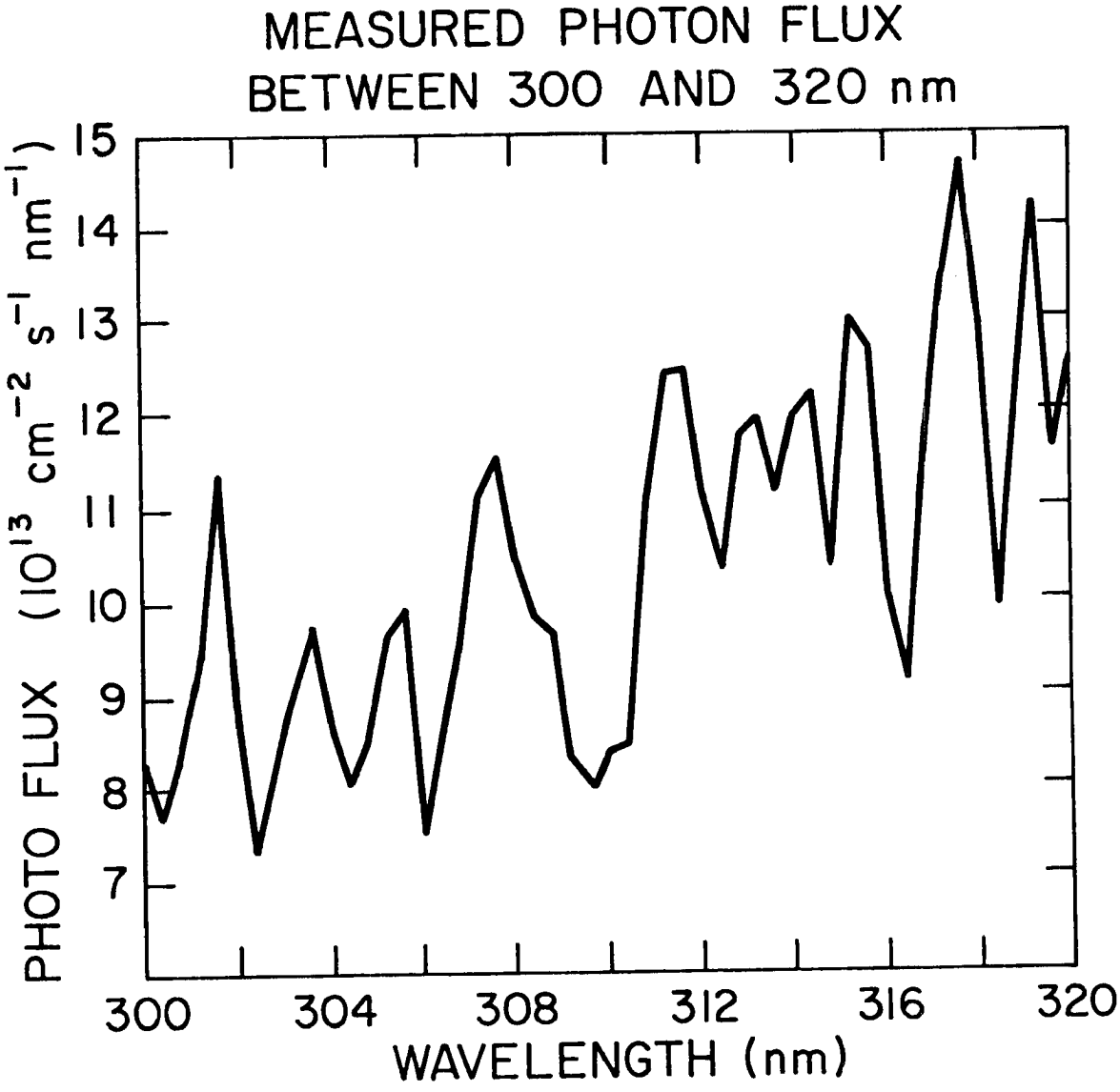

Fig. 16. (from Arvesen et al., 1969)

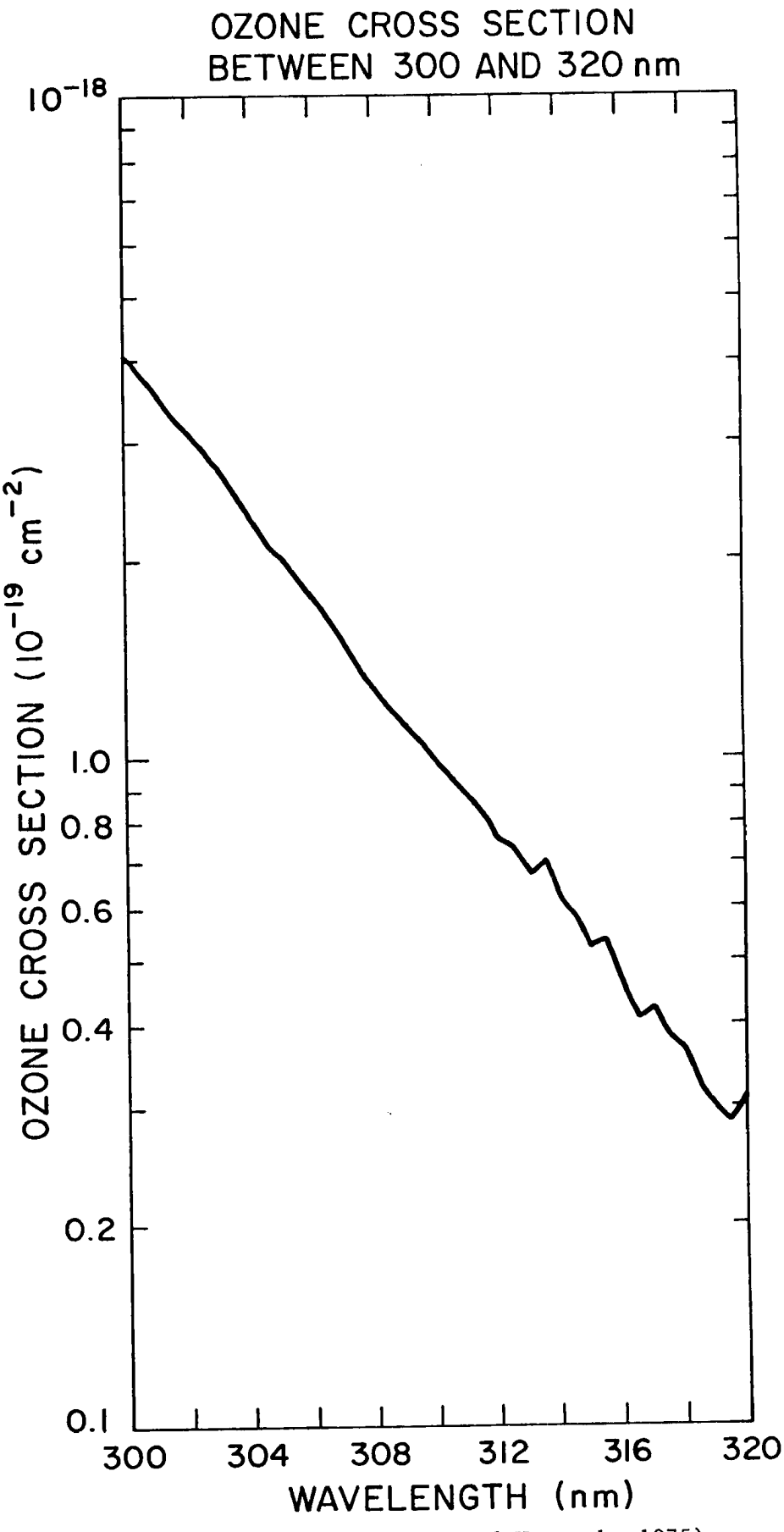

Fig. 17. (from Moortgat and Warneck, 1975)

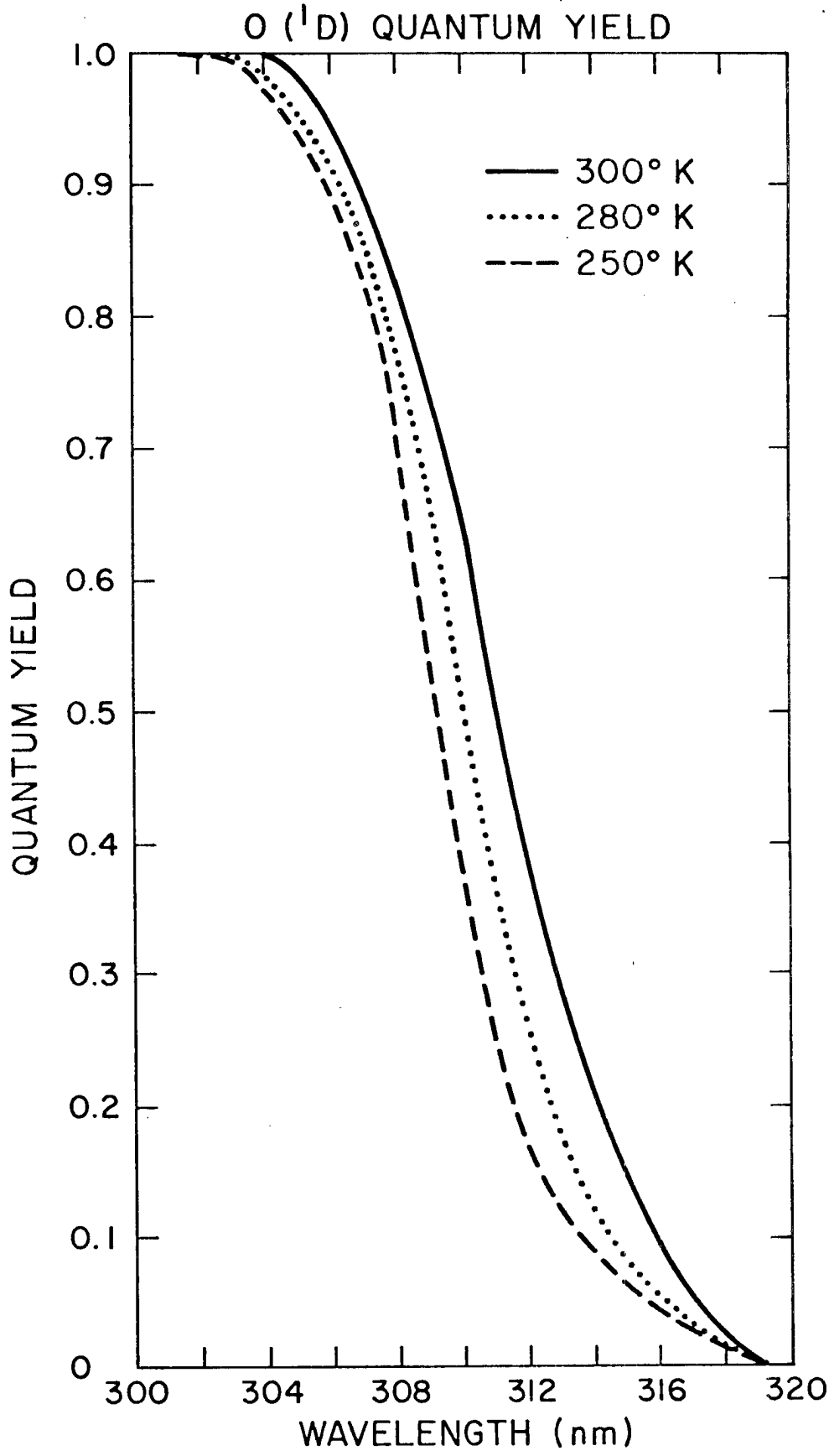

Fig. 18. (from Arnold et al., 1977)

(1969) with a spectral resolution of 0.4 nm. Figure 17 depicts the ozone absorption cross section between 300 and 320 nm (Moortgat and Warneck, 1975). Arnold et al. (1977) have developed an analytical expression for the temperature and wavelength dependence of the $O(^1D)$ quantum yield between 300 and 320 nm. Figure 18 shows these values for three typical ground-level temperatures. The temperature dependence of the quantum yield can alter the calculated production rate of $O(^1D)$ by as much as 20% over the range of tropospheric temperatures.

The model-derived photolysis rates are compared with Dickerson's measurements in Figure 19. The lightly dotted area is the model-derived photolysis rate plotted against the effective ozone column density. The scatter in the calculations exists because of the temperature dependence of the quantum yield and the parameterization of light scattering and absorption at various solar zenith angles. In general, the comparison of the calculated photodissociation rates with the measurements is quite good, and falls within the error bars of the observations for many cases. Overall, the calculated j_{22} is higher than the measured value, especially when the sun is high in the sky (at relatively low values of effective ozone column density). In the particular model calculations shown in Figure 19, the earth's albedo is assumed to be zero and none of the incoming solar radiation is allowed to be attenuated by Mie scattering. In the actual calculations, however, this process was taken into account by assuming an average cloud height in the troposphere centered at 5 kms, and using the albedo data given as a function of latitude and month by Raschke et al. (1973). Note that by incorporating such processes into the calculations shown

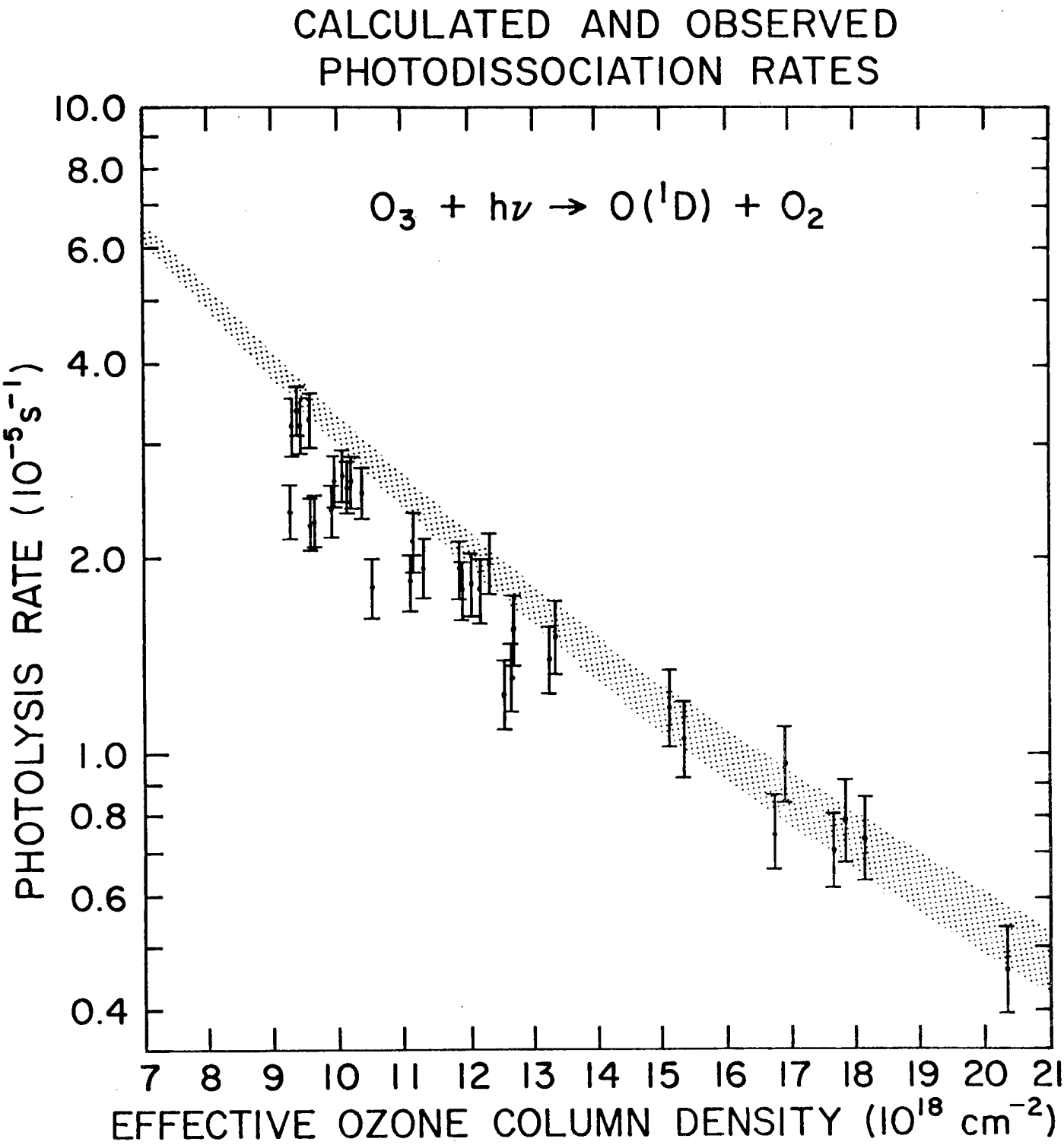
CALCULATED AND OBSERVED
PHOTODISSOCIATION RATES
$O_3 + h\nu \rightarrow O(^1D) + O_2$
PHOTOLYSIS RATE ($10^{-5} s^{-1}$)
10.0
8.0
6.0
4.0
2.0
1.0
0.8
0.6
0.4
7 8 9 10 11 12 13 14 15 16 17 18 19 20 21
EFFECTIVE OZONE COLUMN DENSITY (10^{18} cm^{-2})

Fig. 19

in Figure 19, the model-derived values would be lowered somewhat and might be in better agreement with Dickerson's measurements. In general, however, the model calculations do agree well enough with the measurements that we can conclude that the model is doing a reasonably good job of computing this important photolysis rate.

VIII. SUMMARY AND CONCLUSIONS

Using the global tropospheric distributions of ozone, water vapor, carbon monoxide, temperature and the presently available chemical photokinetic information, we have developed a seasonally varying quasi-steady state numerical model to calculate the distribution of the hydroxyl radical in the troposphere. The resultant tropospheric OH concentration for the globe diurnally averaged over the entire year is approximately 3×10^5 cm^{-3}, which is a factor of two to ten times lower than has been computed directly in previous photochemical models (see Neely and Plonka, 1976). However, this value is consistent with the analysis of methyl cholorform production history and its present global distribution (Singh, 1977a; Chang and Penner, 1977).

In addition to the better agreement with the tropospheric methyl chloroform budget, we showed in Section V that higher average OH values cause Seiler's (1974) carbon monoxide budget to be more out of balance than the lower OH concentrations. Regardless of which OH number densities are correct, an additional source of CO is required to balance Seiler's budget. Furthermore, we showed that the tropospheric budget of ozone may be closely related to the distribution of carbon monoxide and that CO oxidation may be a considerable source of ozone in the Norhtern Hemisphere troposphere. In fact, we conclude from our analyses that the lesser amount of tropospheric ozone seen in the Southern Hemisphere (compared to the Northern Hemisphere) may be a result of the smaller concentrations of CO in the Southern Hemisphere. Ongoing research is looking further into this phenomonen taking into account the possible differences in tropospheric-stratospheric exchange processes in the two hemispheres.

Since ozone enhances OH concentrations and carbon monoxide suppresses them (see Figure 1), the net effect of the CO and O_3 distribution serves to maintain a fairly equal value of OH in both hemispheres. This finding is contrary to the hypotheses of both Crutzen and Fishman (1977) and Singh (1977b) which suggested that OH levels in the Southern Hemisphere could be as much as three times larger than the values in the Northen Hemisphere.

Although we feel in these calculations that examination of the budgets of various trace gases is the best method of determining the validity of the OH distribution, comparison of the model-derived OH number densities with the scattered measurements does not universally refute or support the model results. Compared with our calculated OH values, the measurements of Davis et al. (1976) are several times higher, Campbell's (1977) preliminary observations are slightly lower, and the data of Perner et al. (1976) are too scattered and indeterminate to make a valid comparison. Furthermore, one must realize that a high variability is likely for any particular local OH measurement because of the high variation that exists for the parameters which affect OH directly (e.g., ozone, water vapor, etc.), and that the accuracy of the model cannot be assessed properly unless all important atmospheric parameters are well-known.

In Section VII , we compared our model-derived photolysis rate for the reaction

$$\text{R22}\quad O_3 + h\nu \rightarrow O(^1D) + O_2,$$

with the preliminary measurements of Dickerson. Since this photodissociation rate determines the rate of production of metastable atomic

oxygen, $O(^1D)$, which, through reaction with water vapor, serves as the primary source of OH in the troposphere, a valid comparison of our calculated photolysis rate with the measurements would be indicative of the model's ability to simulate this important rate in the atmosphere. The reasonably good comparison of Dickerson's measurements with our calculations is another sign which suggests that the model's results provide a reasonable approximation of the physical processes taking place in the atmosphere and that the model calculations may yield a fairly realistic picture of the tropospheric OH distribution.

Lastly, a large part of the discussion in this report focuses on the uncertainties involved in the calculations. In particular, the average distributions of the nitrogen oxides (NO and NO_2) in the troposphere and the parameterization of heterogeneous removal processes in the atmosphere are two factors which greatly affect the calculated amounts of OH in the troposphere. This study suggests that very low background levels of NO and NO_2 must be present in the troposphere to yield a reasonable amount of production of tropospheric ozone. The presence of an NO_2 tropospheric column density greater than Noxon's (1977) upper limit of 5×10^{14} molecules cm^{-2} appears to enhance tropospheric photochemical production of ozone through carbon monoxide and methane oxidation to a very high level which exceeds the amount of ozone which can be destroyed in the troposphere by presently known destruction mechanisms. Likewise, through the analysis of various tropospheric budgets, this study shows that a relatively fast heterogeneous removal rate yielding tropospheric residence times of less than half a day for such species as SO_2, NO_2, HNO_3, H_2O_2 and CH_3O_2H is not unrealistic in the troposphere. Until extensive measurements programs

of background levels of NO, NO_2, HNO_3 and H_2O_2 are established and a good understanding of aerosol formation evolves, the incorporation of these parameters into numerical models will remain a source of uncertainty in photochemical calculations.

In conclusion, we feel that in addition to having developed a model which calculates a tropospheric OH distribution, we have provided a comprehensive analysis of the budgets of several trace gases in the troposphere which tends to support this distribution. We have examined some of the more important uncertainties in the model and note that it is not possible to minimize them until more measurements and a better understanding of microphysical processes are available. Lastly, we emphasize that this study should not be looked upon as the final compendium of tropospheric photochemistry, but rather as a first attempt to gain some insights into this complex and important field.

References

Arnold, I., F.J. Comes, and G.K. Moortgat, 1977: Laser flash photolysis quantum yield of $O(^1D)$-formation from ozone, Max Planck Institute for Chemistry, Mainz, preprint.

Arvesen, J.D., R.N. Griffin, Jr., and D.G. Pearson, Jr., 1969: Determination of extraterrestrial solar spectral irradiance from a research aircraft, Appl. Optics, 8, 2215-2232.

Burrows, J.P., G.W. Harris and B.A. Thrush, 1977: The rates of reaction of HO_2 with HO and O studied by laser magnetic resonance, Dept. of Physical Chemistry, Cambridge, U.K., preprint.

Calvert, J.G., J.A. Kerr, K.L. Demerjian and R.D. McQuigg, 1972: Photolysis of fromaldehyde as a hydrogen atom source in the lower atmosphere, Science, 175, 751-752.

Campbell, M.H., 1977: Unpublished data, presented at the Fall, 1977, American Geophysical Union Meeting, December 5-9, 1977, San Francisco.

Chameides, W.L., and D.H. Stedman, 1977: Tropospheric ozone: Coupling transport and photochemistry, J. Geophys. Res., 82, 1787-1794.

Chameides, W.L., D.H. Stedman, R.R. Dickerson, D.W. Rusch and R.J. Cicerone, 1977: NO_x production in lightning, J. Atmos. Sci., 34, 143-149.

Chan, W.H., W.M. Uselman, J.G. Calvert, and J.A. Shaw, 1977: The pressure dependence of the rate constant for the reaction $HO + CO \rightarrow H + CO_2$, Chem. Phys. Ltrs., 45, 240-243.

Chang, J.S., and J.E. Penner, 1977: Analysis of global budgets of halocarbons, submitted to Atmos. Env.

Chang, J.S., and D.J. Wuebbles, 1976: A theoretical model of global tropospheric OH distributions, Proceedings of the Non-Urban Tropospheric Composition Symposium, Hollywood, Fla., jointly sponsored by the Americal Geophysical Union and the Americal Meteorological Society.

Chatfield, R.B., and H. Harrison, 1977a: Troposperic ozone I: Evidence for higher background concentrations, J. Geophys. Res., 82, 5965-5968.

Chatfield, R.B., and H. Harrison, 1977b: Tropospheric ozone II: Variations along a meridional band, J. Geophys. Res., 82, 5969-5978.

Cox, R.A., R.G. Derwent, A.E.G. Eggleton and J.E. Lovelock, 1976a: Photochemical oxidation of halocarbons in the troposphere, Atmos. Env., 10, 305-308.

Cox, R.A., R.G. Derwent, P.M. Holt and J.A. Kerr, 1976b: Photo-oxidation of methane in the presence of NO and NO_2, J. Chem. Soc. Faraday I, 72, 2044-2060.

Crutzen, P.J., 1974: Photochemical reactions initiated by and influencing ozone in umpolluted tropospheric air, Tellus, 26, 47-57.

Crutzen, P.J., and J. Fishman, 1977: Average concentrations of OH in the Northern Hemisphere, and the budgets of CH_4, CO, H_2 and CH_3CCl_3, Geophys. Res. Ltrs., 4, 321-324.

Crutzen, P.J., I.S.A. Isaksen, and J.R. McAfee, 1977: The impact of the chlorocarbon industry on the ozone layer, J. Geophys. Res., in press.

Danielsen, E.F., 1968: Stratospheric-tropospheric exchange based on radioactivity, ozone, and potential vorticity, J. Atmos. Sci., 25, 502-518.

Danielsen, E.F., and V.A. Mohnen, 1977: Project Dustorm report: Ozone measurements and meteorological analysis of tropopause folding, J. Geophys. Res., in press.

Davidson, B., J.P. Friend, and H. Seitz, 1966: Numerical models of diffusion and rainout of stratospheric radioactive materials, Tellus, 18, 301-315.

Davis, D.D., W. Heaps, and T. McGee, 1976: Direct measurements of natural tropospheric levels of OH via an aircraft-borne tunable dye laser, Geophys. Res. Ltrs., 3, 331-333.

Drummond, J., 1977: Atmospheric measurements of nitric oxide using chemiluminescence, Ph.D. Dissertation, Dept. of Physics, Univ. of Wyoming, Laramie.

Dütsch, H.U., 1970: Two years of regular ozone soundings over Boulder, Colo., National Center for Atmospheric Research Technical Note, NCAR-TN-10, Boulder, Colo., 441 pp.

Ehhalt, D.H., 1974: The atmospheric cycle of methane, Tellus, 26, 58-70.

Eliassen, A., and J. Saltbones, 1975: Decay and transformation rates of SO_2, as estimated from emission data, trajectories and measured air concentrations, Atmos. Env., 9, 425-430.

Fabian, P., and P.G. Pruchniewicz, 1977: Meridional distribution of ozone in the troposphere and its seasonal variations, J. Geophys. Res., 82, 2063-2073.

Fishman, J., 1977: A numerical investigation of the meteorological and photochemical processes which influence tropospheric ozone and other trace constituents, Ph.D. Dissertation, Dept. of Earth and Atmos. Sci., Saint Louis University, St. Louis, Mo., 114 pp.

Fishman, J., and P.J. Crutzen, 1977: A numerical study of tropospheric photochemistry using a one-dimensional model, J. Geophys., Res., 82, 5897-5906.

Hampson, R.F., and D. Garvin, 1975: Chemical kinetic and photochemical data for modelling atmospheric chemistry, NBS Tech Note 866, U.S. Dept. of Commerce, 112 pp.

Henmi, T., E.R. Reiter, and R. Edson, 1976: Residence time of atmospheric pollutants and long-range transport, Dept. of Atmos. Sci., Colorado State Univ., Ft. Collins, 78 pp.

Howard, C.J., and K.M. Evenson, 1977: Kinetics of the reaction of HO_2 with NO, Geophys. Res. Ltrs., 4, 437-440.

Isaksen, I.S.A., K.Midtbö, J. Sunde, and P.J. Crutzen, 1976: A simplified method to include molecular scattering and reflection in calculations of photon fluxes and photodissociation rates, Rept. No. 20, Institute of Geophysics, University of Oslo, Norway, 31 pp.

Johnston, H.S., and R.A. Graham, 1973: Gas-phase ultraviolet absorption spectrum of nitric acid vapor, J. Phys. Chem., 77, 62-63.

Junge, C.E., 1960: Sulfur in the atmosphere, J. Geophys. Res., 66, 227-237.

Levy, H., 1972: Photochemistry in the lower troposphere. Planet. Space Sci., 20, 919-935.

Levy, H., 1973: Photochemistry of minor constituents in the troposphere, Planet. Space Sci., 21, 575-591.

Meetham, A.R., 1950: Natural removal of pollution from the atmosphere, Quart. J. Roy. Meteor. Soc., 80, 96-99.

Molina, L.T., S. Schinke, and M.J. Molina, 1977: Ultraviolet absorption spectrum of hydrogen peroxide, Geophys. Res. Ltrs., 4, 580-582.

Molina, M.J., and F.S. Rowland, 1974: Stratospheric sink for chlorofluoromethanes: Chlorine atom-catalysed destruction of ozone, Nature, 249, 810-811.

Moortgat, G.K., and P. Warneck, 1975: Relative $O(^1D)$ quantum yields in the near UV photolysis of ozone at 298 K, Z. Naturforsch, 30a, 835-844.

Moortgat, G.K., E. Kudszus, and P. Warneck, 1977: Temperature dependence of $O(^1D)$-formation in near U.V. photolysis, Max Planck Institute of Chemistry, Mainz, preprint.

NASA, 1977: Chlorofluoromethane Assessment Workshop Report, Goddard Space Flight Center, Maryland.

Neely, W.B., and J.H. Plonka, 1976: An estimation of the time averaged hydroxyl radical concentration in the troposphere, Dow Chemical Co., Midland, Mich., preprint.

Noxon, J.F., 1977: Tropospheric NO_2, J. Geophys. Res., in press.

Perner, D., D.H. Ehhalt, H.W. Pätz, E.P. Roth, and A. Volz, 1976: OH-radicals in the lower troposphere, Geophys. Res. Ltrs., 3, 466-468.

Pittock, A.B., 1974: Ozone climatology, trends and the monitoring problem, Conf. on Structure, Composition and Seasonal Circulation of the Upper and Lower Atmosphere and Possible Anthropogenic Perturbations, Melbourne, Australia, 455-466.

Raschke, E., T.H. Vonder Haar, W.B. Bandeen, and M. Pasternak, 1973: The annual radiation balance of the earth-atmosphere system during 1969-1970 from Nimbus-3 measurements, J. Atmos. Sci., 30, 341-364.

Seiler, W., 1974: The cycle of Atmospheric CO, Tellus, 26, 116-135.

Sie, B.K.T., R. Simonitis, and J. Heicklen, 1976: The reaction of OH with CO, Int. J. Chem. Kin., 8, 85-88.

Singh, H.B., 1977a: Atmospheric halocarbons: evidence in favor of reduced average hydroxyl radical concentration in the troposphere, Geophys. Res. Ltrs., 4, 101-104.

Singh, H.B., 1977b: Preliminary estimation of average HO concentrations in the Northern and Southern hemispheres, Geophys. Res. Ltrs., 4, 453-456.

Söderlund, R., and B.H. Svensson, 1976: The global nitrogen cycle, Nitrogen, Phosphorus and Sulfur--Global Cycles, edited by B.H. Svensson and R. Söderlund, SCOPE Rept. No. 7 and Ecological Bulletin No. 22, Swedish National Science Research Council, Stockholm.

Stolarski, R.S., and R.J. Cicerone, 1974: Stratospheric chlorine: a possible sink for ozone, Can. J. Chem., 52, 1610-1615.

U.S. Standard Atmosphere Supplements, 1966: U.S. Govt. Printing Office, Washington, D.C.

Yung, Y.K., M.B. McElroy, and S.C. Wofsy, 1975: Atmospheric halocarbons: a discussion with emphasis on chloroform, Geophys. Res. Ltrs., 2, 397-399.

BIBLIOGRAPHIC DATA SHEET	1. Report No. CSU-ATSP-284	2.	3. Recipient's Accession No.

4. Title and Subtitle
The Distribution of the Hydroxyl Radical in the Troposphere

5. Report Date
January, 1978

6.

7. Author(s)
Jack Fishman and Paul J. Crutzen

8. Performing Organization Rept. No.

9. Performing Organization Name and Address
Atmospheric Sciences Department
Colorado State University
Fort Collins, Colorado 80523

10. Project/Task/Work Unit No.

11. Contract/Grant No.
EPA-R804921-01

12. Sponsoring Organization Name and Address
Environmental Protection Agency
Environmental Sciences Research Laboratory
Research Triangle Park, North Carolina 27711

13. Type of Report & Period Covered
Project Report

14.

15. Supplementary Notes

16. Abstracts
A quasi-steady state photochemical numerical model is developed to calculate a two-dimensional distribution of the hydroxyl (OH) radical in the troposphere. The diurnally, seasonally averaged global value of OH derived by this model is 3×10^5 cm^{-3} which is several times lower than the number computed previously by other models, but is in good agreement with the value inferred from the analysis of the tropospheric distribution of methyl chloroform. Likewise, the effects of the computed OH distribution on the tropospheric budgets of ozone and carbon monoxide are not inconsistent with this lower computed value.

One important result of this research is the detailed analysis of the distribution of tropospheric ozone in the Southern Hemisphere. Our work shows that there is a considerable difference in the tropospheric ozone patterns of the two hemispheres and that through the analysis of the likely photochemistry occurring in the troposphere, a significant source of tropospheric ozone may exist in the Northern Hemisphere due to carbon monoxide oxidation.

17. Key Words and Document Analysis. 17a. Descriptors

Tropospheric photochemistry
Hydroxyl radical
Ozone Budget
Carbon Monoxide Budget

17b. Identifiers/Open-Ended Terms

17c. COSATI Field/Group

18. Availability Statement	19. Security Class (This Report) UNCLASSIFIED	21. No. of Pages 82
	20. Security Class (This Page) UNCLASSIFIED	22. Price